https://ntrs.nasa.gov/search.jsp?R=19740011329 2020-03-17T14:29:05+00:00Z

N74-19442

6. Determination of Meteor Parameters Using Laboratory Simulation Techniques

J. F. Friichtenicht and D. G. Becker
TRW Systems Group
Redondo Beach, California

Atmospheric entry of meteoritic bodies is conveniently and accurately simulated in the laboratory by techniques to be described which employ the charging and electrostatic acceleration of macroscopic solid particles in the 0.02 to 1 μ diameter range. Velocities from below 10 to above 50 km/s are achieved for particle materials which are elemental meteoroid constituents (e.g.: Fe, Si, Mg) or mineral compounds with characteristics similar to those of meteoritic stone (e.g.: $FeTiO_3$). The velocity, mass, and kinetic energy of each particle are measured nondestructively, after which the particle enters a target gas region. Because of the small particle size, free molecule flow is obtained at target pressures ≦10 torr. At typical operating pressures (0.1 to 0.5 torr), complete particle ablation occurs over distances of 25 to 50 cm; the spatial extent of the atmospheric interaction phenomena (luminous trails, ionized wakes, etc.) is correspondingly small, simplifying many experiments. Procedures have been developed for measuring the spectrum of light from luminous trails and the values of fundamental quantities defined in meteor theory: heat transfer coefficient λ, drag coefficient Γ, ionization probability β, and photographic luminous efficiency τ_{pg}. Results of these measurements are presented, with emphasis on recent, improved evaluations of τ_{pg} and β over wide velocity ranges; it is shown that the laboratory values of τ_{pg} for iron are in excellent agreement with those for 9 to 11 km/s artificial meteors produced by rocket injection of iron bodies into the atmosphere. Also discussed in some detail is the relevance of these measurements to the interpretation of meteor observations and the methods of inferring from them numerical values of τ_{pg} and β for natural meteors.

Simulated meteors, in the sense that we shall use the term, are phenomena which occur when macroscopic particles of known composition are accelerated to meteoric velocities *in the laboratory* and then injected into simulated "atmospheres" of known gas composition and density. These may be contrasted with artificial meteors, which are created by rocket injection of manmade bodies into the Earth's atmosphere. In this paper we intend to limit ourselves to a discussion of laboratory meteor simulation techniques and experiments, referring to artificial meteor experiments and to natural meteor observations only to compare results. We do not intend to imply by this decision that meteor simulation is generally superior to the other two methods; rather, we regard each of them as having its own unique advantages and each as being most suitable in turn in different experimental contexts.

Initially received with caution and some skepticism, laboratory meteor simulation is now beginning to be recognized as an experimental

technique of much potential value for attacking a number of unresolved or poorly resolved problems in meteor physics, certain of which have proven stubbornly unyielding to conventional observational methods. For fundamental measurements of basic meteor processes, this technique possesses two very important advantages. One is that it frees the experimenter from the necessity of waiting upon nature: It makes it possible for him to create "meteors" in the convenience of his own laboratory, in any desired quantity, and with all variables under his complete control. The other is that it enables him to separate complex meteor interactions into individual components more easily examined. As an example, he may choose to employ monoconstituent particles or monoconstituent atmospheres, changing the constituents one by one and thereby obtaining basic data from which the interaction of a multiconstituent meteoroid with a complex atmosphere may, hopefully, be synthesized. The price paid for these advantages is that the experimenter accepts the burden of demonstrating that the simulation is a meaningful approximation to a natural meteor and of developing methods for achieving the desired synthesis. These are questions that we plan to deal with later at length.

A key factor affecting the accuracy of the simulation is the flow conditions in the atmospheric gas. Most meteor phenomena appear in the extreme upper atmosphere, where low density results in free molecule flow. It is readily shown that to produce free molecule flow under practical laboratory conditions, particle size should be quite small. Calculations of mean free path as a function of pressure indicate that a 1-μ diameter particle experiences free molecule flow at pressures as high as several torr, and at such pressures a meteor is produced with a total trail length of a few tens of cm. A 1-cm diameter particle, on the other hand, requires gas pressures below about 10^{-3} torr for free molecule flow, and then the meteor which it produces will have a trail length measured in kilometers, far too long to be contained in reasonable laboratory apparatus.

Besides being small in size, the particles must obviously attain meteoric velocities; optimally, particles should be available at any and all velocities between 10 and 70 km/s. These considerations rule out light gas guns and other ballistic accelerators. Of the available microparticle hypervelocity systems, only electrostatic acceleration presently appears to combine small particle size with truly meteoric velocities. The latter technique provides in addition a large, continuous flux of particles, which allows considerable volumes of data to be acquired in a relatively brief operating time.

Early efforts to accelerate microparticles to hypervelocities began in the late 1950's and were largely motivated by a desire to study possible impact and erosion damage to spacecraft that might result upon their passage through the "dust cloud" that was then thought by many to encircle the Earth. Shelton et al. (1960) developed a method of electrically charging micron-sized spherules of a conducting powder by contact and succeeded in accelerating them in an electrostatic field. They also developed detectors that utilized the particle charge to provide nondecelerative measurement of the mass, velocity, and lateral position (with respect to the flight axis) of each particle. Friichtenicht (1962) adapted the Shelton particle charger to a commercial 2 MV Van de Graaff proton accelerator, obtaining thereby a conveniently operated research tool capable of accelerating 1μ diam iron microparticles to velocities up to about 15 km/s. This is the basic facility still employed for meteor simulation; it has, however, been further improved through the introduction of newer particle detectors developed by Hansen and Roy (1966) and time-of-flight coincidence techniques employing special instrumentation described by Roy and Becker (1971). These improvements have significantly increased the signal-to-noise ratio for particle detection, and their use has revealed the formerly unsuspected presence of numerous submicron-sized particles with velocities in the 50 km/s range in the Van de Graaff "beam." A second approach to higher particle velocities has been to increase the accelerating voltage. Becker et al. (1965) have described a linear accelerator to accomplish this; the linac became operational in 1967, but to date it has proved most useful in other types of experiments and will not be discussed further.

Until fairly recently, carbonyl iron and carbon black were the only commercially-available powders with properties suited to the Shelton particle charger. Since iron is a major meteoroid con-

stituent, the early meteor simulation experiments were conducted almost exclusively with this material. But within the last few years there have occurred major advances in the manufacture of fine powders which have greatly increased the number of usable particle materials. Some of these are also meteoroid constituents, some are of interest for purposes of comparison, and some are compounds similar to certain components of meteoritic stone.

Although, as we have noted, microparticle acceleration was first developed to create an experimental tool for cratering and erosion studies, it was observed during the early 1960's that when a hypervelocity microparticle entered a low-pressure gas environment, it produced a luminous trail visible to the naked, dark-adapted eye. The similarity to natural meteor phenomena was obvious, and this observation provided the impetus for attempts to simulate meteors. The first detailed laboratory study of the interaction of high velocity microparticles with gases was performed by Slattery, Friichtenicht, and Hamermesh (1964). They examined deceleration, particle heating, and production of luminous trails, and experimentally determined values for the drag coefficient Γ and heat transfer coefficient λ as defined in meteor theory for velocities from below 4 to 6–7 km/s. Later, Friichtenicht, Slattery, and Tagliaferri (1968) measured the luminous efficiency of iron particles interacting with air at velocities from 20 to 35 km/s, and Friichtenicht (1969) determined the heat transfer coefficient in this velocity regime. Detailed spectral measurements of the iron luminosity were also performed by Tagliaferri and Slattery (1969). Finally, recent experiments by Becker and Friichtenicht (1971) have resulted in a more accurate evaluation of iron luminous efficiency over the entire velocity range from 11 to 47 km/s. These new data can, as we shall see, be directly compared over part of the velocity spectrum with results obtained by other methods, and such a comparison supplies important evidence regarding the accuracy of the simulation process. Becker and Friichtenicht also measured the luminous efficiency of copper from 11 to 47 km/s, thereby laying the groundwork for an understanding of the relationship between luminous efficiency and particle composition.

The discovery that visual and photographic meteors could be simulated led to attempts to simulate the ionized wakes of radiometeors. Such wakes were found to exist in the laboratory. They were studied in the specific meteor context by Slattery and Friichtenicht (1967), who found values for the ionization probability of simulated iron micrometeors entering air and argon atmospheres at 20 to 40 km/s, and in a more general context of collisional ionization theory by Friichtenicht, Slattery, and Hansen (1967). These measurements were extended by Friichtenicht and Becker (1971) to copper at 16 to 38 km/s and to lanthanum hexaboride at 20 to 112 km/s; the latter values are important to the understanding of collisional ionization processes involving compounds and to the behavior of the phenomenon at high velocities.

In the following discussion we will review in detail the laboratory techniques that are employed in these and other simulated meteor experiments. We will also examine the most recent results that have been obtained in our programs of measurement of the important meteor parameters. We hope to demonstrate from those results that, as we have long believed, these laboratory techniques do in fact provide a meaningful and accurate simulation of natural meteor processes.

TECHNIQUES FOR MICROPARTICLE ACCELERATION AND DETECTION

Since meteor simulation ultimately depends upon the ability to accelerate microparticles and to measure their parameters after acceleration, let us begin by examining the equipment and techniques that fulfill these functions. We will also consider certain accessory instrumentation which provides greater control over the accelerated particles and/or improves the signal-to-noise ratio for particle detection.

It was seen in the introduction that the meteor simulation process is based upon the particles being electrically charged. This charge is imparted to them by the device shown in figure 1, which we term a "particle injector" (since it injects the charged particles into the accelerating field) and which is identical in concept to the injector first constructed by Shelton et al. (1960). The principal components of the injector are the powder reservoir, the tongue, and the charging chamber;

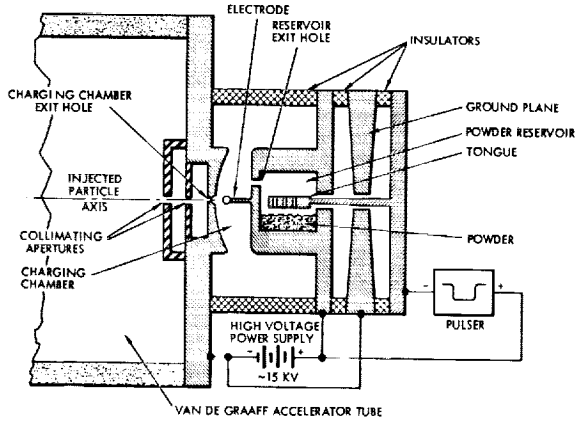

FIGURE 1.—Simplified diagram of particle injector. With no pulse applied to tongue, powder remains at rest. When tongue is pulsed negatively, powder is set in motion. Some particles diffuse through reservoir exit hole and enter charging chamber. There they eventually come in contact with electrode tip, which is at high field. On contact the particle receives a high charge, and the fields propel it out through the chamber exit hole and collimating apertures. Ground plane creates high fields along tongue shaft to inhibit backward diffusion of powder.

the latter includes a needle-like charging electrode and a shaped ground plane containing an exit aperture. Normally the powder reservoir and the tongue above it are both maintained at a positive potential of ~15 kV, the reservoir is field-free, and the powder is at rest. When particles are to be charged, the tongue is pulsed toward ground for a few milliseconds. This imposes an electric field within the reservoir, under whose influence the powder is set into violent motion. A number of particles will diffuse through the reservoir exit hole and will find themselves in the charging chamber. (Diffusion of particles backward along the shaft supporting the tongue is discouraged by high fields in this region.) In the chamber particles oscillate back and forth between the surfaces, exchanging charge at each surface and moving essentially as they would if specularly reflected. The shape of the chamber is such that particles move inward toward the charging electrode, whose tip has been formed into a ball with a diameter comparable to that of the particles. The electrode tip is obviously a region of very high field. When a particle contacts this tip, it receives a correspondingly high charge and is then propelled by this field through the chamber exit hole. Note that the entire procedure takes place *in vacuo*.

The injector will normally be mounted on the end of the accelerator tube of the 2 MV Van de Graaff (Friichtenicht, 1962). Each injected particle is then accelerated through the full potential across the tube. The injector design is such that the electrostatic focusing system present in the Van de Graaff (which, it will be recalled, was originally designed for use with a proton or positive ion source) functions normally. At a distance of a meter or so from the Van de Graaff baseplate, the particle "beam" can be focused to a diameter on the order of 2 mm. This "beam" is not continuous, but instead consists of from one to a few hundred particles for each tongue pulse applied to the injector. Pulsing of the injector is controlled by circuitry in the Van de Graaff control console and in the high voltage terminal of the machine; these are coupled by insulated rods originally present in the Van de Graaff as purchased and by a pulsed light beam system developed by us for this purpose. The potential applied to the charging electrode, the amplitude of the tongue pulse, and the pulse repetition rate can all be adjusted from the control console. Varying the pulse amplitude determines the number of particles injected with each pulse. The repetition rate can be set at any of six fixed values from 10 to 600 pulses/minute, or the injector may be pulsed manually by a pushbutton. The high particle flux is a very important feature of the system, since it results in a short data acquisition time—especially when, as will be seen, only a small fraction of the total flux is usable in the experiment.

It is evident that the operation of the particle injector depends upon the conducting properties of the powder with which it is filled. It was once thought that the powder must be a good conductor, but more recent research has shown that materials with bulk resistivities as high as about 10^{10} ohm-cm can be employed. Other important requirements for a usable powder are that it flow readily, to prevent agglomeration and subsequent clogging of the injector apertures and to insure that single particles, rather than clumps, are charged, and that its particles be reasonably uniform in size. Table 1 lists those materials which have so far been successfully tested. The table is

by no means exhaustive and is limited almost entirely by the time available in which to try different materials. Included in the list are three of the major metallic constituents of meteoritic stone: silicon, iron, and aluminum. The fourth, magnesium, has not yet been tested, but the properties of this metal are so similar to those of aluminum that little difficulty is expected in its use. Not all of the tabulated materials have been used extensively enough for us to acquire detailed data on their performance. For those that have been, we list in table 2 the maximum velocities that have been measured and the corresponding particle masses and radii. It is clear that most materials attain velocities in the neighborhood of 50 km/s, and that this value is considerably exceeded in a few cases.

TABLE 1.—*Materials Usable for Contact Charging and Acceleration*[a]

Metallic elements	Intermetallic elements	Alloys	Compounds
Ag	C	316 stainless steel[b]	$CaTiO_3$[b]
Al	Si		CrB
Co[b]			$FeTiO_3$
Cu			LaB_6
Fe			MoB
Ni			NiAl
Ta[b]			PbTe
Ti[b]			SiC[b]
U			TiC[b]
W[b]			TiN[b]
			TiO[b]

[a] Includes only materials actually tested as of January 1971.

[b] Materials so noted have been bench-tested in standard injectors; all others have been accelerated by the Van de Graaff as well.

We may now examine the factors that determine accelerator performance in more detail. A particle with a total charge q and a mass m that has been accelerated through a potential V_a attains a velocity v given from energy conservation as

$$v = \left(2\frac{q}{m}V_a\right)^{1/2} \tag{1}$$

First, the Shelton injector charges all particles to a constant surface field intensity, and so the charge q should be proportional to particle area, or equivalently to r^2 where r is the particle radius. (We assume here that the particles are spherical.) Since the mass m is proportional to r^3, we would expect v to vary as $r^{-1/2}$. Actual data for iron (the material which has been used for the longest time and for which we have the most complete data) are presented in figure 2, where the quantity $v/V_a^{1/2}$ has been plotted as a function of r. The data deviate somewhat from the theoretical behavior predicted by Shelton et al. and can instead be approximated by the expression

$$v/V_a^{1/2} = 4.6\times10^{-3}\,\rho^{-1/2}r^{-3/4} \tag{2}$$

in which ρ is the particle density (7.85×10^3 kg/m^3 for iron) and all units are MKS. Our experience with other materials tends to indicate

TABLE 2.—*Maximum Velocities Achieved for Various Particle Materials Accelerated Through 1.5 MV*

Material	Velocity (km/s)	Mass (kg)	Radius (microns)
Aluminum	54.8	4.28×10^{-19}	0.034
Carbon	35.0	1.80×10^{-18}	0.058
Chromium boride (CrB)	50.7	4.26×10^{-19}	0.025
Copper	48.7	3.62×10^{-19}	0.021
Iron (carbonyl)	68.6	3.52×10^{-19}	0.022
Iron metatitanate ($FeTiO_3$)	43.4	3.51×10^{-19}	0.026
Lanthanum hexaboride (LaB_6)	112.0	9.94×10^{-20}	0.021
Lead telluride (PbTe)	39.3	7.06×10^{-19}	0.027
Molybdenum boride (MoB)	55.7	1.92×10^{-19}	0.018
Nickel aluminide (NiAl)	71.6	1.68×10^{-19}	0.019
Silicon	50.3	5.47×10^{-19}	0.038
Silver	30.8	7.98×10^{-19}	0.026

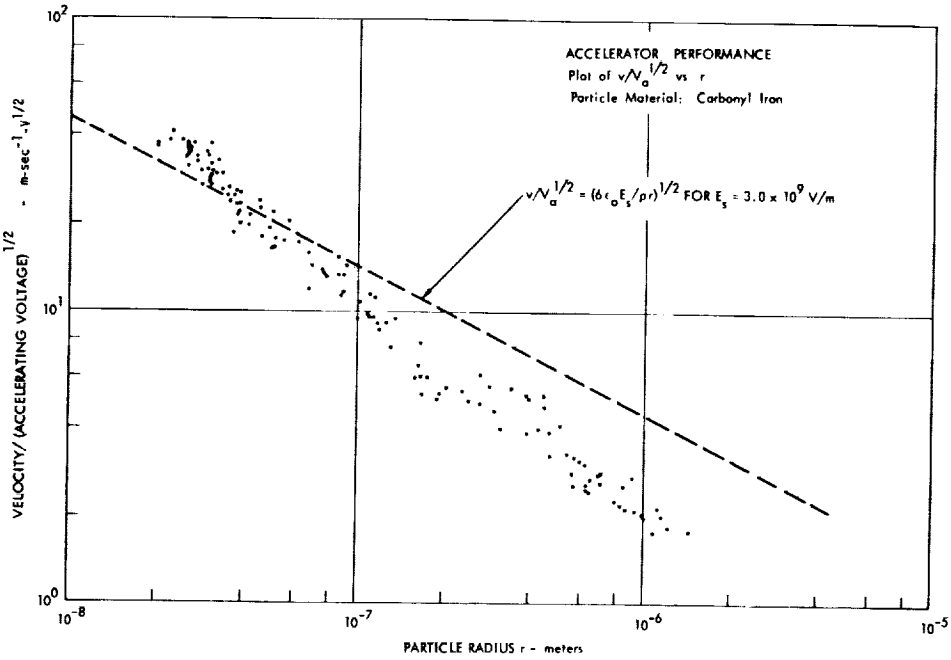

FIGURE 2.—Plot of $v/V_a^{1/2}$ vs r for iron particles. Straight line is theoretical relationship proposed by Shelton et al. (1960); data are actually proportional to $r^{-3/4}$.

that they generally follow equation (2) except for a constant factor. These data show that the highest velocities are attained by the smallest particles, and this is the reason why a powder should contain particles of sufficiently uniform size to at least exclude larger, more massive particles that would attain relatively low velocities. Another consequence of the data follows from our remarks about the relationship between charge and radius. Although the highest velocity particles have the highest charge-to-mass ratios, they also have the lowest absolute value of charge. They are therefore the hardest to detect, which accounts for the fact that these small, fast particles were not even known to be present until steps were taken to improve the signal-to-noise ratio for particle detection.

A basic particle detector appears in figure 3(a). The detector consists of three concentric tubes, the outer two being grounded with the inner one connected to a charge-sensitive preamplifier. When a charged particle enters this structure, it induces an equal charge on the inner tube which remains for only as long as the particle is actually within the inner tube. This induced charge is amplified as a voltage signal by the preamplifier. The preamplifier output, seen in figure 3(b), is a square pulse whose amplitude is proportional to particle charge q and to the ratio C_i/G, where C_i and G are the capacitance to ground of the detector structure and the preamplifier gain, both of which are known constants. The width of the pulse is of course inversely proportional to particle velocity and depends otherwise only on the known length of the inner tube. (The grounded outer tubes remove fringing effects and insure that the edges of the pulse are sharp.) Knowing the charge, velocity, and accelerating potential, the particle mass can be computed from equation (1); if the particles are spherical and their density is known, the radius is easily found.

Two other useful types of particle detector can be seen in figure 3. In figure 3(c), the inner tube has been split into two parts, between which is placed a system of horizontal and vertical plates. This detector produces a four-part output signal. On passage of a particle through the tubes, the signal has an amplitude proportional to q as before. However, the signal in the regions of the plates is also proportional to the distance between the particle flight axis and the grounded plate; a particle whose flight axis coincides with the de-

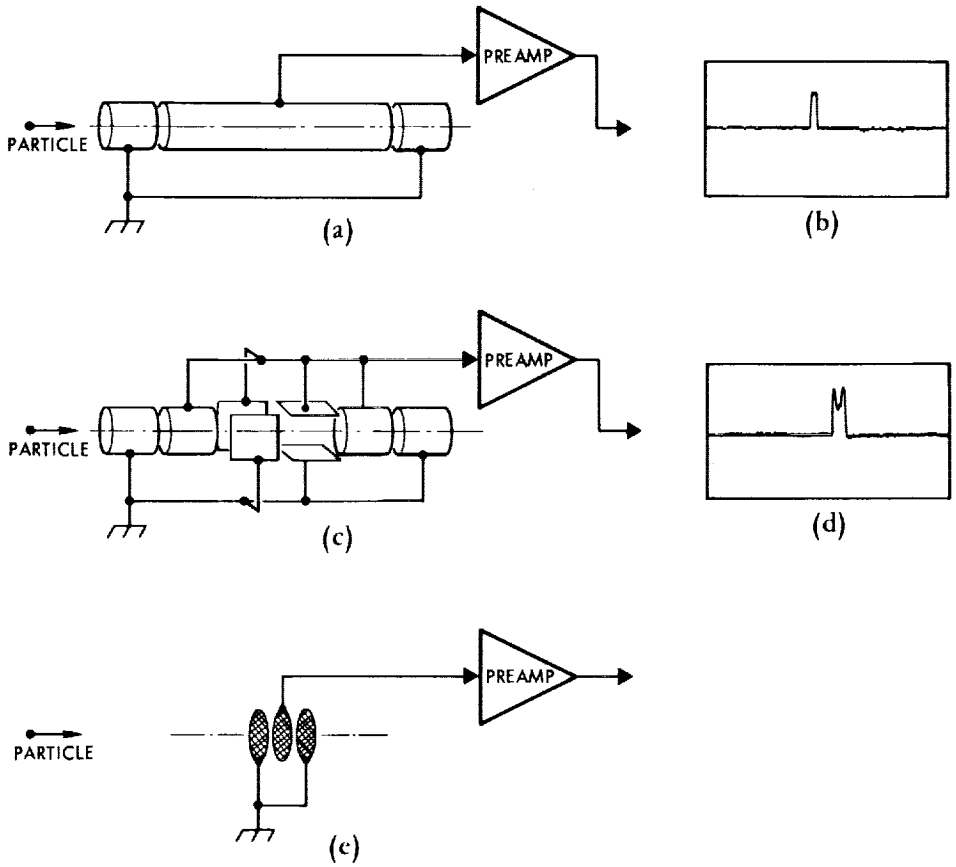

FIGURE 3.—Three types of particle detectors, with some representative output signals. (a) Detector for charge and velocity measurement. (b) Output signal from (a); amplitude is proportional to particle charge and width to transit time through the central tube. (c) Detector for lateral position measurement. (d) Output signal from (c); ratio of inner to outer parts of composite pulse gives lateral position with respect to horizontal and vertical axes; particle is centered when ratio = 0.5. (e) Timing mark detector, with tubes replaced by close-spaced grids; output is a sharp pulse whose peak coincides with particle passage through the central grid.

tector symmetry axis produces a signal whose amplitude is half that from the tubes. A typical composite output signal is shown in figure 3(d), and it is clear that this signal permits one to determine the lateral position of the particle in two coordinates. Such detectors are employed for focusing (by adjusting until the lateral positions of all particles are the same) and for system alignment (by moving the detector and other apparatus until the particles are centered in the detector bore). In figure 3(e), the detector inner tube has degenerated to a screen. A particle entering this detector produces a narrow pulse as it passes the screen, which can be used as a position marker. A pair of such detectors placed a known distance apart form a time-of-flight range for accurate particle velocity measurement.

It can be shown that the signal-to-noise ratio for particle detection is proportional to $C_i^{-1/2}$, which implies that the detector input capacitance must be made as small as possible. This is achieved in part mechanically and in part electronically by the "bootstrapped" preamplifier developed by Hansen and Roy (1966). The grid detector of figure 3(e) has an especially low structural capacitance and is therefore attractive in timing operations with small, high velocity particles.

Selection of Particle Parameters

We have found that it is essentially impossible to obtain powders with particle size variations less than about two orders of magnitude. A typical powder usually contains particle radii from about 1 or 2μ down to perhaps 0.02μ, and further size sorting is impractical. (Particles with radii greater than a few microns can be eliminated and should be, unless there is a specific reason for working with relatively massive low-velocity particles.) According to figure 2, the velocities of particles charged and accelerated from such a powder mix will vary over a wide range. In principle, if one is performing an experiment covering a wide velocity spectrum, one can simply accept all particles at random, relying on the velocity distribution inherently resulting from particle size variations to cover the range. In practice, however, low velocity particles will predominate, both because of their greater actual number and the fact that their larger signals will be much more prominent in the detectors. (Remember that large, slow particles have a higher absolute value of charge.) Therefore, in many cases it would be preferred that all of the instrumentation in an experiment respond only to particles with velocities in a specified range. Additionally, there arise instances in which out-of-range particles may unduly perturb the experiment, and then it is necessary to physically prevent the unwanted particles from interacting. Equipment has been developed to fulfill all of these functions, and the presence of this equipment has become essential to the proper operation of most simulated meteor experiments.

Several different means have been employed to achieve selection of desired velocities. The one in current use is the time interval selector and proportional delay generator discussed by Roy and Becker (1971); the reader is referred to their paper for a detailed description of the workings of this instrument. Operationally, it functions as follows: Two inputs are provided, which are connected to the outputs of a pair of particle detectors of the type in figure 3(c), assembled as a time-of-flight range. The instrument examines the flight time of all particles passing through this range. When it is determined that a given measured flight time lies within the range for which the instrument is preset, then and only then are a series of output-trigger pulses generated. One pulse appears instantaneously as soon as the flight time measurement is completed, and the others are separately delayed in time by a multiple or submultiple of the measured flight time; the multiplying factors are constants and can be set by the experimenter to any value between 0.1 and 10.0. A little thought will show that these proportional delays appear when the particle has reached a given point in space irrespective of the particle velocity. One of the two delays may be used to trigger a downstream charge detector [of the type shown in fig. 3(a)] just as the particle reaches it, and the other is usually used to trigger the instrumentation that records interaction effects just as the particle enters the experimental region. In this way, not only is data acquisition limited to a preset velocity interval, but also flight-time coincidence is introduced. That is, all downstream instrumentation is active only for that brief time in which a desired particle is expected, which reduces the effective bandwidth for data recording and thereby lowers the effective system noise level. Without such coincidence techniques, many of the small, fast particles would not be observed.

The fact that the particles are charged makes it relatively easy to remove unwanted particles from the "beam." A transverse electrostatic field can be used to deflect all particles away from a suitable aperture. When a desired particle appears, the time interval selector output trigger causes the removal of the field for a time sufficient to permit the desired particle to pass undeflected. Figure 4 illustrates the simple scheme that we have employed to accomplish this. A pair of parallel plates is installed along the particle flight path. The passive plate is held at a low dc voltage, and the active plate is connected both to a high-voltage dc power supply and to the plate of a pulse tube which is biased at cutoff. The potential difference between the plates is then almost 10 kV, and if the plates are 10 to 15 cm long, the transverse field is more than ample to deflect all particles away from the exit aperture, whose diameter is about 1 cm. When a trigger pulse is received from the time interval selector warning that an in-range particle is about to enter the deflector, the trigger activates a pulse generator.

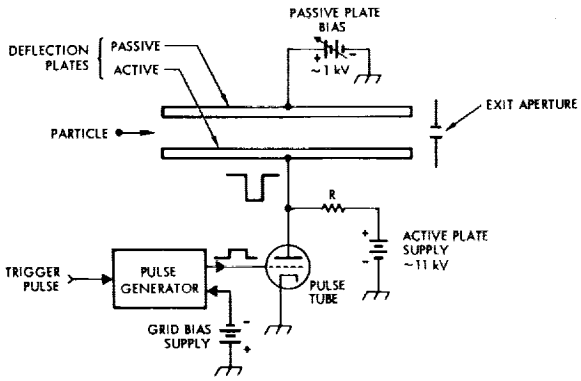

FIGURE 4.—System for controlled particle deflection. Pulse tube is normally in cutoff and 10-kV potential difference appears across deflection plates; all entering particles are deflected from exit aperture. When a trigger arrives signaling the approach of an acceptable particle, pulse generator applies a positive pulse to tube grid, causing current to be drawn through R and dropping the active plate potential to ~1 kV so that particle passes undeflected. Passive plate bias is adjusted for zero residual deflection of acceptable particles.

This unit produces a positive pulse whose width is set to exceed the time required for the particle to pass completely through the plates and whose amplitude is sufficient to drive the pulse tube into saturation. The pulse is applied to the pulse tube grid, causing current to be drawn in the plate circuit so that almost all of the supply voltage is dropped across plate resistor R. The active plate thus falls to a low voltage, which is equal to the small dc voltage on the passive plate. (The latter voltage is determined by experiment, adjusting it until there is no residual deflection of acceptable particles.) The transverse field between the plates hence drops to zero until after the desired particle has passed.

There occasionally arise a few experiments in which it is desired that all particles have almost the same mass. Equation (1) shows that the particle mass can be controlled by limiting both the particle velocity and the charge. Since the latter is proportional to the amplitude of the particle detector output signal, it can be controlled simply by feeding this signal through an appropriate window discriminator that generates an output trigger only if the amplitude lies within the limits of the window. This trigger and the one from the time interval selector are combined in a coincidence circuit; if and only if both triggers are present, the circuit turns off the particle deflector.

Integration of the Equipment Into a Facility

In figure 5, all of the equipment described above has been combined and assembled to form the basic meteor simulation facility. By now the operation of the various parts of this facility will be familiar. Particles are charged in the particle injector, accelerated and focused by the 2 MV Van de Graaff, and then enter the analysis region. There they encounter a pair of detectors set up as a time-of-flight range. The detector outputs are fed to the time interval selector and proportional delay generator, which searches for particles with in-range velocities. If mass selection is desired, the time-of-flight range is immediately followed by a charge detector connected, as we have seen, to a window discriminator. The undelayed output of the time interval selector and the window discriminator output are combined as previously discussed in a coincidence circuit, whose output triggers the deflector. Downstream from the deflector is another particle charge detector. Its output will be recorded and employed later to compute the actual particle mass and velocity prior to its entrance into the experimental region. Data recording is generally by a multitrace oscilloscope operated in the single-sweep mode and fitted with a trace-recording camera. One oscilloscope trace is triggered by the first proportionally-delayed trigger from the time interval selector unit; this trigger always occurs at position x_1, located just before the entrance to the charge detector. The second trace records the data from the experimental interaction; it is triggered by the second proportionally-delayed trigger when the particle reaches position x_2. The second delay multiplying factor is adjusted to make location x_2 coincide with the point in space where the interaction under study first begins.

There are several possible variations to the basic system, depending upon the nature of the experiment. The first charge detector, window discriminator, and coincidence circuit are of course omitted when, as in the majority of experiments, mass selection is unnecessary. The deflector may also be omitted if out-of-range particles will not disturb the experiment. (In any event, data from

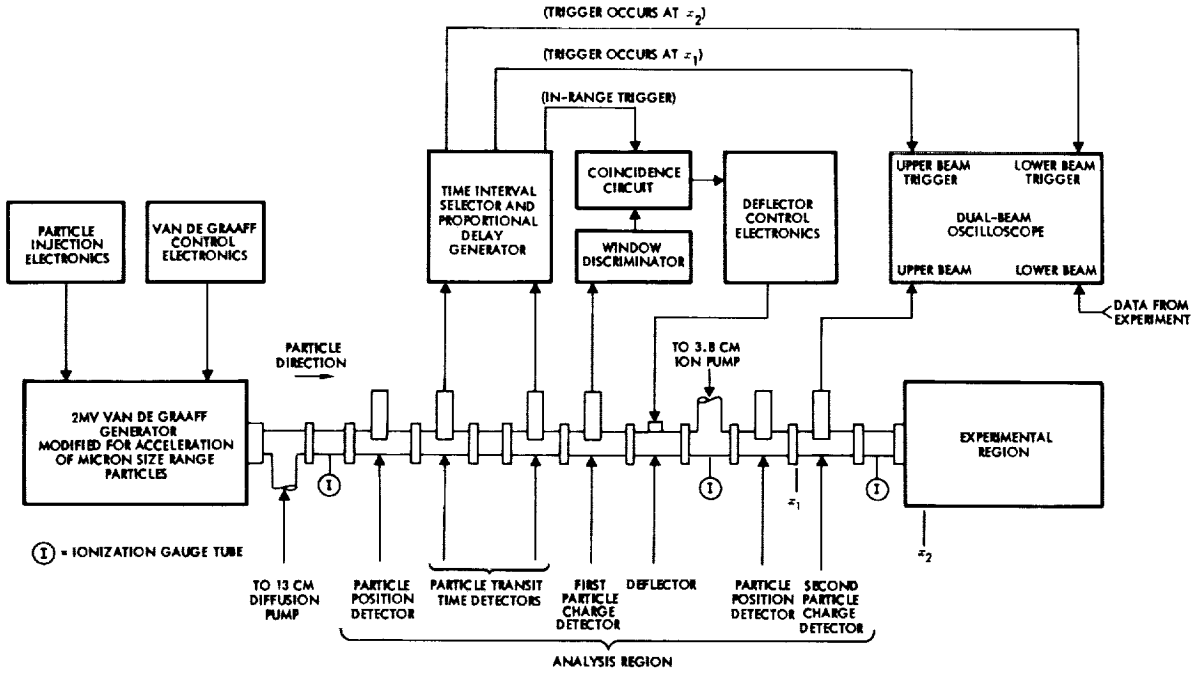

FIGURE 5.—Facility employed for simulated meteor experiments; see text for functions of major components and modifications used in certain cases. Position detectors are used only for initial alignment and focusing of the particle "beam."

such particles will not be recorded because the data recording oscilloscope will not have been triggered.) Finally, it has been observed in certain instances that if the vacuum in the analysis region is not sufficiently good, some particles may lose charge during their passage through the analysis region. Any loss of charge results in a false mass measurement and is to be avoided. If we suspect that this phenomenon is likely to occur in a given case, we often replace the single downstream charge detector with two detectors spaced a considerable distance apart and determine the charge from both detector outputs. When the values disagree, the datum is rejected.

The vacuum within the analysis region, the Van de Graaff accelerator tube, and the particle injector is maintained in the 10^{-5} to 10^{-6} torr range by a 13 cm (nominal 4-in. size) oil diffusion pump assisted by a 3.8 cm ion pump.

Data Reduction System

Because of the large volume of data generated in most of our simulated meteor experiments, we have developed a system of semiautomatic data reduction. We showed above that the raw data are usually contained in one or more oscilloscope trace photographs. The traces include the detector signal [fig. 3(b)] whose amplitude and width must be reduced to particle charge and velocity, and also various other signals containing data relating to the interaction under study. Reduction of the latter almost always involves measurement of one or more pairs of time/amplitude coordinates. The photographs are placed in a Telereader* unit, which projects them onto a screen with a pair of X-Y movable crosshairs. When these crosshairs are moved, their positions are continuously digitized in the Telereader; the origin for the position coordinate system can be set by the experimenter to coincide with an appropriate feature of the oscillogram. The experimenter moves the crosshairs so as to measure the particle detector signal width and amplitude and the coordinates of interest in the interaction signal.

* Registered trademark.

When each measurement is complete, the digitized data are automatically transferred to punch cards, each of which is simultaneously tagged with an identifying number in order that a given interaction and the parameters of the specific particle producing it are always uniquely correlated. The completed card deck is then fed to a high-speed digital computer where the data are operated on and combined with supplied constants. For each particle and its corresponding interaction, the computer prints out particle velocity, charge, mass, energy, radius, and momentum, and the interaction data reduced to meaningful physical units and normalized, if desired, to any of the particle parameters the experimenter may select.

This system has most of the advantages of fully automatic data acquisition, requiring as it does only manual read-in of the data. We regard this too as an advantage, however, because it enables the experimenter to utilize his own scientific judgment in determining whether any given datum may be spurious and in deciding how a given oscillogram must be interpreted. Our experiences with complete automation in which individual data cannot be judged indicates that such systems are less than satisfactory and can introduce serious errors.

INSTRUMENTATION FOR SIMULATED METEOR MEASUREMENT

Having seen how microparticles are accelerated to meteoric velocities, controlled, and detected, we next must investigate how these particles are made to create a simulated meteor and how the properties of the meteor may be measured. It is apparent that the particles must interact with a gaseous environment in order that a meteor be produced. As we have already seen that the analysis phase of the particle flight occurs *in vacuo*, it follows that the first problem is to introduce the particle into a downstream gas region without deteriorating the upstream vacuum. Simultaneously, the pressure and composition (if other than air) of the target must be controllable. Finally, the results of the particle-gas interaction must be observed, recorded, and measured; in all of the experiments to be discussed later, the result to be observed is either photon emission or ionization.

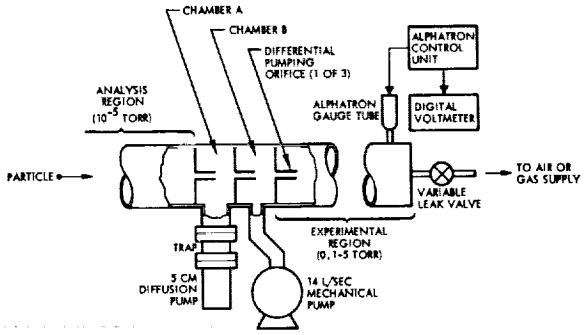

FIGURE 6.—Sketch of differential pumping and target gas control systems. If the pressure in the experimental region is to be below 1 torr, chamber B and the mechanical pump can be eliminated.

A differential pumping system is employed to allow the particles to make a transition from high vacuum to gas. The system is shown schematically in figure 6. The analysis region and the experimental region are separated by two intermediate chambers linked by small orifices. The chamber nearest the "gas" side of the system is pumped by a 14 l/sec mechanical pump, and the one nearest the "vacuum" side is connected to a trapped 5-cm oil diffusion pump. The orifices connecting the chambers are designed to have gas conductances much lower than the pumping speeds of the pumps. (Typical orifice dimensions are 1.3 to 2.5 mm diameter and 2.5 to 5 mm length.) Gas is admitted to the experimental region through a precision variable leak valve. The pressure in this region is carefully monitored, usually by an Alphatron* vacuum gauge whose control unit has been modified to digital voltmeter readout for greater accuracy and which has been calibrated against a McLeod gauge. If the pressure in the experimental region is to be less than about 1 torr, the mechanically-pumped chamber can be dispensed with. Because of the small orifice diameter through which all particles must pass, excellent focus of the particle "beam" and good axial alignment of the orifices with the "beam" axis are essential.

None of the simulated meteor phenomena that we have studied to date have shown any particular dependence on absolute gas pressure, although we have always investigated for the possible presence

* Registered trademark.

of such effects. Therefore, adjustment of the gas pressure is not especially critical, provided that it is known and that two limits are observed. The upper limit is set by the requirement that the particle experience free molecule flow. Suppose we assume, conservatively, that free molecule flow ceases when the mean free path ℓ in the gas falls below $10d$, where d is the particle diameter. If the gas molecules are approximated by rigid spheres, the mean free path and gas pressure p are shown in standard texts (cf. Hirschfelder et al., 1954) to be related according to

$$\ell = \frac{kT}{1.3p\sigma} \tag{3}$$

where k is Boltzmann's constant, T the absolute temperature, and σ the gas kinetic cross section, generally approximated as 3×10^{-15} cm^2 for air. Using this expression with $T=300°$ K, $\ell=10d$, and $d=1\mu=10^{-4}$ cm, we find that $p=8$ torr. This, then, is the upper pressure limit. The lower pressure limit is set merely by the fact that the meteor phenomenon must be completely contained within the experimental apparatus, since data analysis is considerably simplified when it is known that particle ablation has been complete and that the meteor has been observed over its entire length. The minimum pressure that produces this condition is most easily found by trial and error; it is typically on the order of 0.1 torr for fast, small particles in air, rising to perhaps 0.5 torr for 1μ diameter particles at $\sim$10 km/s.

The phenomenon of meteor luminosity is generally studied through the use of one or more photomultiplier tubes (PMT) placed transverse to the particle flight axis. Since the luminous trails of the smaller particles are quite faint, the PMT's must be sensitive. They must also cover the entire spectral range of interest, which in our experiments has been the photographic meteor spectrum from 3300 Å to 5200 Å. We have obtained satisfactory service from RCA types 8575 and 6199, Centronic type P4242B, and one or two others. Our PMT windows are generally acrylic plastic, which has a sharp cutoff at 3400 Å. (This is close enough to the edge of the photographic spectrum for most purposes.) Again because of the very low light intensities, it is necessary to integrate the photocurrent at the PMT anode in order to obtain usable signals. We therefore measure total light energy rather than intensity, and our data analyses must take this into account.

Figure 7 shows the simple setup that we employ to measure the total light energy radiated from a simulated photographic meteor. Note that two PMT's are used, each viewing the luminous trail through a long window, and that one PMT has markers placed in its field of view to block the light as the meteor passes behind the marker. It is clear that neither PMT integrated output directly measures the total radiated energy, since the solid angle subtended by the PMT at the instantaneous particle position is small and is also constantly changing. However, a theoretical relationship can be derived between the PMT output signal and the total radiated energy which permits one to compute the latter after measuring the fraction of the energy collected at the time that the meteor disappears behind the marker. Another feature of the setup is that an additional delayed pulse from the time interval selector-proportional delay generator (see fig. 5) is generated at position x_3 near the end of the chamber. This pulse is added to one of the PMT outputs and serves to insure that the meteor has terminated, i.e., that all possible light has been collected, before it passes

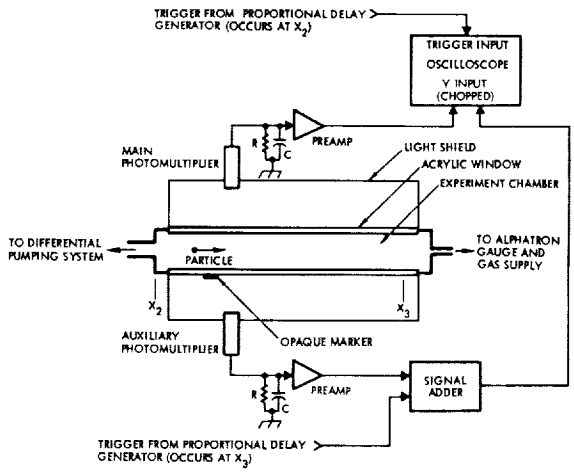

FIGURE 7.—Equipment employed for the measurement of total light energy radiated by a simulated meteor. Photomultiplier (PMT) signals are integrated by resistors R and capacitors C at the PMT anodes; the RC time constant is typically $\sim$500 μsec. Opaque marker and auxiliary PMT are used to obtain data for a solid angle correction, as discussed in the text and by Becker and Friichtenicht (1971).

out of view of the PMT's. (We require, for a datum to be valid, that there be no further increase in the PMT output signal after the appearance of the marker pulse.) Figure 8 is a typical oscillogram obtained from this setup.

Most experiments in which luminosity is the observable require that the spectrum of emitted light be known. We measure spectra using the system indicated in figure 9. Here up to six PMT's view the luminous trail simultaneously, all providing identically integrated outputs. Five of the tubes are fitted with narrow-band interference filters and the sixth is left unfiltered. The peak amplitude of any filtered PMT output normalized to the output of the unfiltered tube gives the relative amount of light emitted within the filter bandwidth. These data can be averaged for numerous simulated meteors in a given velocity interval. Using commercial filters, we obtain relative spectral intensity measurements at 300 Å intervals within the photographic meteor spectrum. Our data analysis requires only the integral of the relative spectrum, and as the integral is fairly insensitive to spectral changes, these measurements are sufficiently accurate for our needs.

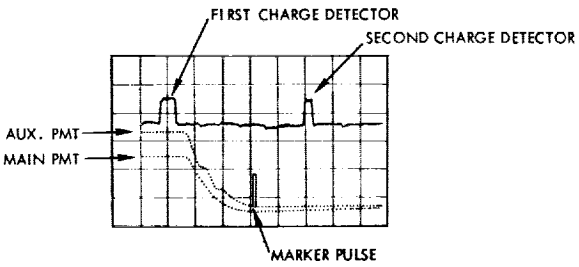

FIGURE 8.—Typical oscillogram obtained from equipment shown in figure 7. Top trace is particle detector signal; two charge detectors were used here with their outputs added, and velocity can be found from the transit time between them. Lower traces are the PMT outputs "chopped" together; these begin when particle is at x_2 and delayed marker appears when particle is at x_3. Steps on auxiliary PMT trace are produced by opaque markers (see text and fig. 7). For this simulated meteor, all sweep speeds were 10 μsec/division; deflection factors were 0.02 V/division and 0.05 V/division for the first and second charge detectors, 1.0 V/division for both PMT outputs, and 5.0 V/division for the marker pulse.

When the experiment deals with the ionized wake of a simulated radiometeor, we change to the ionization chamber setup displayed schematically in figure 10. There are actually two ionization chambers in linear sequence, each having 9-cm wide parallel plates separated by 5 cm and fitted with secondary suppression grids. The plates are equally and oppositely biased so that the particle flight axis lies in the zero equipotential plane. Charge-sensitive preamplifiers can be connected

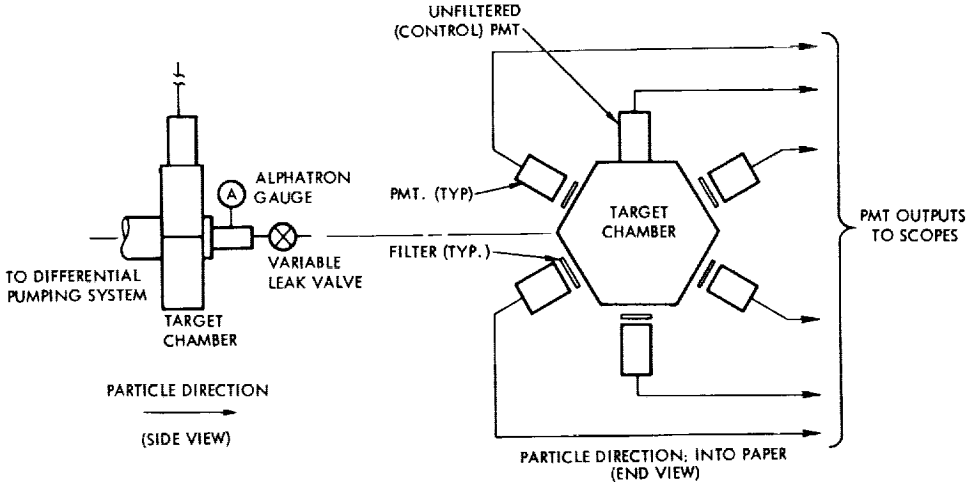

FIGURE 9.—Equipment for the measurement of simulated meteor spectra. Each PMT output is separately integrated and has an appearance similar to the main PMT trace in figure 8. Relative spectrum is derived from ratios between emitted light in passband of each filter and total emitted light as measured by unfiltered PMT.

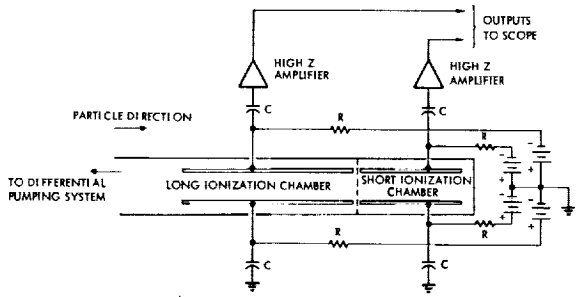

FIGURE 10.—Equipment for the measurement of ionization probability. Long ionization chamber collects all positive and negative charges in meteor wake; total number of positive charges is found from the output of the preamplifier. Short chamber checks length of the wake; any charges collected in it signify excessive wake length, and such data are rejected.

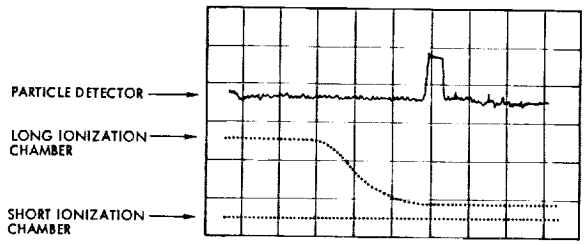

FIGURE 11.—Typical oscillogram obtained from equipment shown in figure 10. Note that short ionization chamber produced no signal, implying that this datum is acceptable. For particle charge detector trace, sweep speed was 5 μsec/division and deflection factor was 0.02 V/division; for ionization chamber traces, corresponding values were 5 μsec/division and 2.0 V/division.

either to the negative plate for measurement of total positive ion charge, or to the positive plate for measurement of total electron and negative ion charge. The former connection is most often used in order to avoid problems that might arise from the short electron collection time and possible production of secondaries; the "unused" plate is ac grounded by capacitors. The preamplifiers are similar in many respects to those employed in particle detection. They integrate the total charge collected at the plate, providing a proportional output voltage whose peak amplitude is in effect proportional in turn to the total number of collected ions (assuming, as is expected at the energies involved, that all ions are singly charged). The first ionization chamber has plates 45 cm long and serves for the actual data acquisition. The second chamber, with 22 cm long plates, is installed to determine whether the first chamber has collected all of the charge in the wake: The presence of any signal in the second chamber is regarded as grounds for rejection of the datum.

As before, the outputs of the ionization chamber preamplifiers are fed to an oscilloscope whose sweep is started by the time interval selector-proportional delay generator when the particle reaches position x_2 at the entrance to the first chamber. A typical oscillogram appears in figure 11.

EXPERIMENTAL RESULTS

Our researches to date have been largely concentrated on those aspects of the meteor problem which appear to meet two informal criteria. The first is obvious—the phenomenon under study should be one for which accurate data are lacking and/or interpretation of existing data is controversial, and for which our techniques seem to have a reasonable probability of supplying the missing data or resolving the controversy. The second is more subjective—we require that our techniques compare favorably with possible alternative research methods in terms of data returned per unit time or per unit expenditure. These considerations have guided our work toward the following areas of study: (a) luminosity effects, including measurements of luminous efficiency and the spectra of luminous trails; (b) ionization effects, particularly the measurement of ionization probabilities for various combinations of particle and atmosphere compositions; (c) other particle-gas energy exchange mechanisms, notably ablation and deceleration, and measurement of drag and heat transfer coefficients. Within the specific context of meteor simulation, those experiments that can be grouped under (c) are probably farthest from fulfilling our self-imposed criteria and will receive the least emphasis in the discussion to follow. Nevertheless, such experiments are still important, since a knowledge of ablation and deceleration mechanisms applicable to these particular particles is necessary to the reduction and analysis of data obtained from experiments in the other two groups.

In the introduction we alluded to a fourth experimental problem, which is to determine the

limits of accuracy of the simulation process and of the extrapolation of results to natural meteors. This problem is difficult to deal with directly, but much indirect evidence can be derived from the experiments themselves. In general, we feel that confidence can be placed in the relevance of the experimental results to the degree that the postulated deceleration and ablation mechanisms yield reasonable results for the drag and heat transfer coefficients, and to the degree that the results can be shown to agree with those obtained by other experimental means.

Deceleration and Ablation

Details of the deceleration and ablation processes have been studied by Slattery et al. (1964), Friichtenicht (1969), and Hersh et al. (1969). These studies employed air, oxygen, and argon atmospheres with carbonyl iron as the particle material. The sphericity of these particles has been verified numerous times by microscopic examination, permitting us to use the spherical shape factor in all data analyses with confidence. The studies have left little doubt that deceleration becomes negligible above 15–25 km/s, that the particles ablate by vaporization from about 10 km/s to the upper extremes of velocity, and that other ablation mechanisms such as sputtering and fragmentation are not important. Additional supporting data for the latter conclusion are visual and photometric observations of luminous trails and computations by Öpik (1958, ch. 5 and 6). In all cases the oxygen results are quite consistent with those for air.

The drag coefficient Γ in our usage is the same as that defined in conventional meteor theory. Under free molecule flow conditions and with all particles assumed spherical, the meteor drag equation is

$$m(dv/dt) = -\Gamma A \rho_a v^2 \qquad (4)$$

where m, v, and A are the mass, velocity, and projected area of the particle, and where ρ_a is the density of the gas with which it interacts. All drag experiments have been conducted at velocities low enough that particle heating by gas molecule bombardment is insufficient to produce significant mass ablation; then m and A remain constant at their initial values $m_0 = 4\pi r_0^3 \rho/3$ and $A_0 = \pi r_0^2$, where r_0 is the initial particle radius and ρ is the particle density. If the particle enters the gas at time $t=0$ with an initial velocity v_0, the velocity at time $t=\tau$ is given by integration of equation (4):

$$\frac{1}{v} = \left[\Gamma \rho_a \left(\frac{9\pi}{16} \frac{1}{m_0 \rho^2}\right)^{1/3}\right] \tau + \frac{1}{v_0} \qquad (5)$$

If x is the distance travelled by the particle from $t=0$ to $t=\tau$, a second integration gives

$$x = \left[\Gamma \rho_a \left(\frac{9\pi}{16} \frac{1}{m_0 \rho^2}\right)^{1/3}\right]^{-1} \times \ln\left\{\left[\Gamma \rho_a \left(\frac{9\pi}{16} \frac{1}{m_0 \rho^2}\right)^{1/3}\right] v_0 \tau + 1\right\} \qquad (6)$$

Note that in equations (5) and (6), all quantities within the square brackets are constant for any one material.

Slattery et al. (1964) used a series of particle velocity detectors within the gas region to obtain the velocity of a decelerating particle as a function of time. Particle parameter measurement prior to gas entry gave m_0 and v_0; ρ_a was found from gas pressure measurements, with the absolute gas pressure held in the area of 1 torr to insure free molecule flow. Naturally, ρ was known (7.85×10^3 kg/m^3 for iron particles). For each particle, reciprocal velocity was plotted as a function of time and a best-fit straight line was prepared by the method of least squares. The slope of this line was equal to the quantity in square brackets in equation (5), and from the slope Γ was determined. Data were obtained for ten particles interacting with air at initial velocities between 4.0 and 6.7 km/s. A total of 17 additional data points were also obtained with an oxygen atmosphere and 12 with argon; the latter results were very similar to those for air and require no further discussion.

Hersh et al. (1969) measured the total particle flight time between two detectors spaced apart a distance x and reduced their data according to equation (6). They employed an air atmosphere only, but in all other respects the experiment was essentially identical to that outlined above. Over 100 particles were observed, with initial velocities ranging from about 0.8 to 3.5 km/s.

In figure 12, drag coefficient data from both experiments are plotted together as a function of

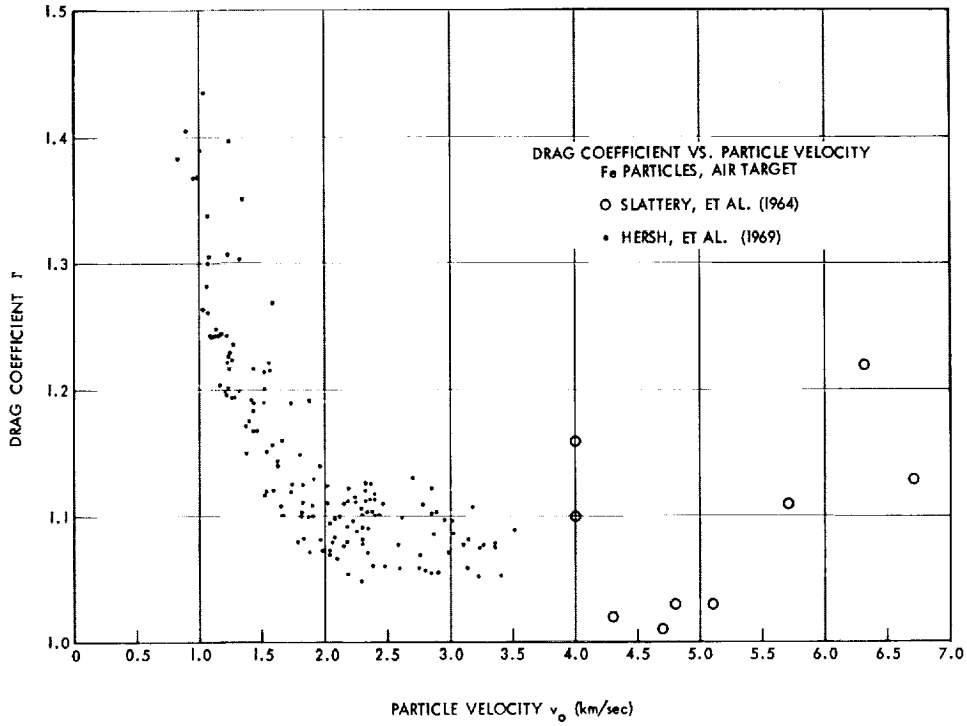

FIGURE 12.—Drag coefficient Γ as a function of initial particle velocity v_0. Data are from Slattery et al. (1964) and Hersh et al. (1969). The better controls and more refined techniques in the latter experiment resulted in a much smaller degree of scatter.

initial velocity v_0. The principal significance of these data in the context of meteor simulation is that Γ tends toward unity as v_0 approaches the lower limit of meteoric velocities, a result consistent with the assumption of particle sphericity and in agreement with the drag coefficient deduced for natural meteors from observations and other deceleration experiments (cf. Whipple and Hawkins, 1959). Hersh et al. have also related their work to details of the particle-gas molecule collision process as contained in theoretical models of free molecule flow and have found good agreement with the models; the interested reader is referred to their paper for further information.

Slattery et al. also measured a heat transfer coefficient for low velocity iron particles. In their experiment, as we have noted, there was insufficient particle heating to produce mass ablation, but the particle did acquire sufficient internal energy to melt. It was possible to determine the time at which melting was complete by examining the behavior of the particle charge, and therefore the total time τ from entry into the gas to melting could be measured. The heat transfer coefficient Λ for melting could then be determined by balancing the energy required to raise the particle temperature 1500° K to the melting point against the internal energy input from gas molecule collisions. If C is the specific heat of iron,

$$m_0 C(1500) = \tfrac{1}{2}\Lambda A_0 \rho_a \int_0^{\tau} v^3\, dt \qquad (7)$$

As in the drag experiments, initial velocity v_0 and mass m_0 were found from a particle parameter measurement just prior to gas entry, and v was obtained as a function of time by direct measurement in the gas. A_0 was computed from m_0 in the usual way, assuming spherical, constant-density particles. Data were obtained for 13 particles entering an air atmosphere at $3.8 \leq v_0 \leq 6.7$ km/s and for additional particles entering oxygen and argon atmospheres.

At meteoric velocities the particle of course ablates, and we return to the definition of the heat transfer coefficient λ given in meteor theory by the

energy-balance equation

$$\zeta(dm/dt) = \tfrac{1}{2}\lambda A \rho_a v^3 \qquad (8)$$

in which ζ is the heat of ablation. The expected result for natural meteors is that complete ablation occurs with relatively little deceleration. This is also true for simulated meteors with $v_0 \geq 20$ km/s or so (as we will later verify by computation). If we limit ourselves to particles with this velocity or greater, we can let $v = v_0 =$ constant. However, A varies as the particle ablates away. If x is the position coordinate of the ablating particle measured along its trajectory with $x = 0$ at entrance into the gas, it is clear that $A/A_0 = f(x)$. Then, if ablation is complete at some position x_f, equation (8) requires that

$$\lambda = 2\zeta m_0/\rho_a v_0^2 \int_0^{x_f} (A/A_0)\, dx \qquad (9)$$

Friichtenicht (1969) designed an experiment to measure λ for 25 to 40 km/s iron particles in air utilizing the principles outlined above. The experimental problem reduces to evaluation of the integral in equation (9), and to accomplish this Friichtenicht observed the luminous trail with instrumentation like that in figure 7. The integrated PMT output (see fig. 8) is proportional to the total radiated energy as a function of time, which can be shown from standard meteor luminosity theory to depend only upon m/m_0. Since the particles do not decelerate appreciably, the time scale can be converted directly to x, and the data are plots of m/m_0 vs x. But $A/A_0 = (m/m_0)^{2/3}$, and hence each particle datum is readily transformed to a plot of A/A_0 vs x from which the integral in equation (9) can be computed.

There remains the problem of specifying a value for ζ. Friichtenicht reasoned that for relatively dense particles of this size range, vaporization is the most likely ablation mechanism. Therefore, in his experiment he set ζ equal to the sum of the heats of fusion and vaporization of iron. He argued that a particle with an unpolished surface in free molecule flow should have $\lambda \approx 1$ (Öpik, 1958, pp. 52–54); if his results gave a λ near unity, this would tend to confirm that the assumption of vaporization as the primary ablation mechanism was correct.

Friichtenicht's measurements of λ for 50 iron particles are combined with those of Slattery et al. in figure 13. It is seen that the heat transfer coefficient is approximately unity for melting at low velocities and declines slightly for ablation at higher velocities. These results appear to be reasonable and tend to support the hypothesis of vaporization as a primary ablation mechanism. Combined with the drag data, they also support the contention that deceleration and ablation processes of simulated meteors are similar to those undergone by natural meteors.

Before leaving this subject, we would do well to reconsider, in the light of the values given above for Γ and λ, whether our assumption of negligible deceleration for an ablating particle with $v_0 \geq 20$ km/s is correct. Dividing equation (8) by (4) and integrating the result from $v = v_0$ to a final velocity $v = v_f$, we obtain the familiar expression

$$m_f = m_0 \exp\left[-\tfrac{1}{2}\sigma(v_0^2 - v_f^2)\right] \qquad (10)$$

where m_f is the residual mass when $v = v_f$ and σ, the ablation constant, is equal to $\lambda/2\Gamma\zeta$. Table 3 gives values of the fractional velocity change $(v_0 - v_f)/v_0$ computed from equation (10) for 99 percent mass ablation ($m_f/m_0 = 0.01$) at various initial velocities. Deceleration can clearly be ignored for v_0 greater than 20 to 25 km/s. In the 10 to 20 km/s range, deceleration is moderate but must be considered.

Luminosity

Because of the fact that so much of our information regarding natural meteors has been obtained by photographic observations, there is considerable interest in both the atomic-scale mechanisms of meteor light emission and the macroscopic-scale relationships existing between the emitted light and the gross properties of the meteoroid. Advances in the quantum theory of atomic collisions have led to a reasonable understanding of the former, although detailed calculations are very complex. Ideally, the latter can be derived theoretically from computations of the populations of all possible excited states if the constituent elements of the meteoroid are known. In practice, the effort is heroic in scope and has apparently been attempted only by Öpik (1933, 1955); his results come very close to certain others derived from observations, but, perhaps because of the complexity of their derivation, they have usually been regarded as somewhat tentative

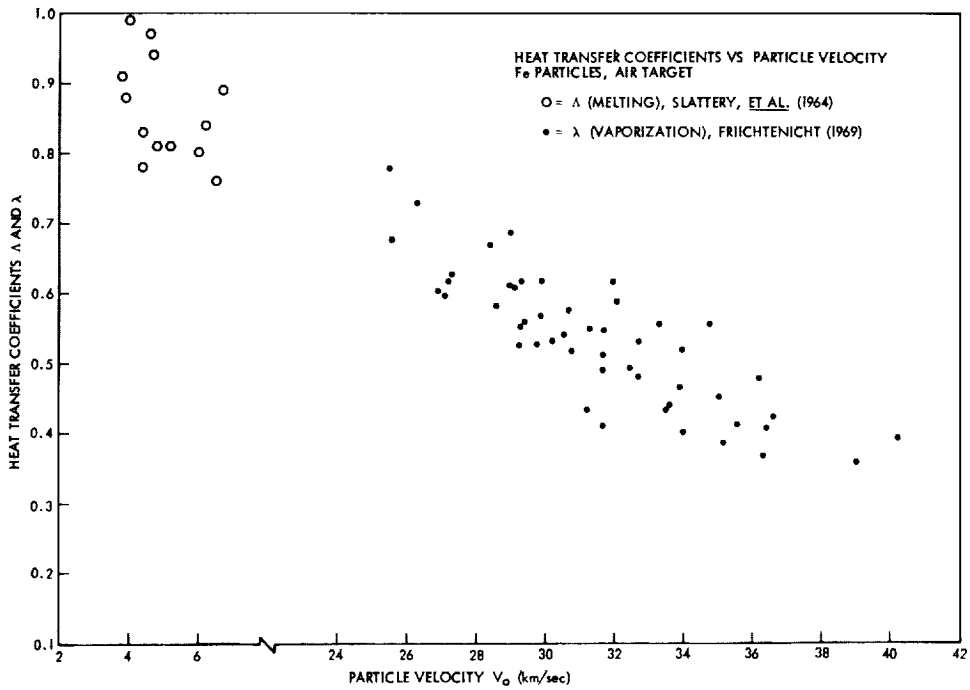

FIGURE 13.—Plot of the heat transfer coefficients Λ for melting and λ for ablation as functions of initial particle velocity v_0. Data are from Slattery et al. (1964) and Friichtenicht (1969).

TABLE 3.—*Deceleration for 99 Percent Mass Ablation* ($m_f/m_o = 0.01$)

Initial velocity (km/s)	Final velocity (km/s)	Fractional velocity change
40.0	38.4	0.04
30.0	27.7	0.09
25.0	22.2	0.11
20.0	16.4	0.18
15.0	9.7	0.35

and in need of more positive experimental verification. Primary emphasis seems instead to have been placed on observation and experiment. Meteor luminosity has been studied in this manner by numerous workers, including notably Verniani (1965), who statistically analyzed a large number of Harvard Meteor Project observations, and Ayers et al. (1970), who report results from artificial meteor experiments first introduced by McCrosky and Soberman (1963). Simulated meteor luminosity experiments were initially performed by Friichtenicht, Slattery, and Tagliaferri (1968). Their work has been improved and extended by Becker and Friichtenicht (1971), whose results we will present below.

As we know, a fraction of the kinetic energy of atoms ablated from a meteoroid is converted into atomic or molecular excitation and eventually into radiation. That fraction is the luminous efficiency of the meteor. It is generally more convenient to deal only with the portion of the radiation which is sensed by a detector with specified spectral response characteristics. The detector of major interest is a meteor camera with blue-sensitive astronomical film, whose combined spectral response has been claimed by Davis (1963) to closely approximate that of the International Photographic System. According to tabulations by Allen (1955), developed from a detailed study by Seares and Joyner (1943), the spectral response function $P(\lambda)$ in this system extends from 3300 to 5200 Å, with a peak at 4600 Å. The energy balance between the radiant intensity I_{pg} observed by a detector with a response function $P(\lambda)$ and the kinetic energy of the ablated atoms is expressed by the meteor

luminosity equation:

$$I_{pg} = -\tfrac{1}{2}\tau_{pg} v^2 dm/dt \qquad (11)$$

in which τ_{pg} denotes the photographic luminous efficiency. If τ_{pg} is accurately known and if a meteor observation measures I_{pg} and v as functions of time, then, by integrating the luminosity equation, these data can be used to solve for the initial meteoroid mass (called the photometric mass when computed in this way). It is evident that the accuracy of photometric mass computations is ultimately limited by the accuracy to which τ_{pg} is known.

If valid, the luminosity equation implies a principle with important consequences for the interpretation of simulated meteor experiments which was, to our knowledge, first pointed out explicitly by Becker and Friichtenicht in their 1971 paper. Assume that the elemental constituents of a meteoroid are well mixed and that the body ablates uniformly. In such a case the relative abundances of the various constituents remaining in the unablated body are constant during the ablation process. This means that if A_k is the initial relative abundance of some constituent k and if m_k is the total mass of that constituent, then the relation $m_k = A_k m$ holds not only initially, but also throughout meteoroid ablation, as a result of which $dm_k/dt = A_k\, dm/dt$. The total luminous intensity I_{pg} of the meteor can be theoretically thought of as a sum of radiant intensities $I_{pg}(k)$, each arising from deexcitation of ablated atoms of one constituent, and it is possible to write a luminosity equation for each such constituent individually, viz.:

$$I_{pg}(k) = -\tfrac{1}{2} A_k \tau_{pg}(k) v^2\, dm/dt \qquad (12)$$

where $\tau_{pg}(k)$ is the luminous efficiency of constituent k. Let all equations of this kind be summed; the left side of the sum, $\Sigma I_{pg}(k)$, must equal I_{pg}. But if this is so, the right side of the sum must equal the right side of equation (11), and we have that

$$\tau_{pg}(M) = \sum_k A_k \tau_{pg}(k) \qquad (13)$$

in which $\tau_{pg}(M)$ denotes the luminous efficiency of the meteor as a whole. We conclude that $\tau_{pg}(M)$ can be evaluated as a weighted sum of luminous efficiencies of those constituent elements which contribute to the radiation within the photographic spectral range. Fortunately, meteor spectra (cf. Millman, 1963) have already identified these elements as iron, silicon, magnesium, and occasionally calcium, and their relative abundances in meteoritic stone are fairly well known (cf. Öpik, 1958, p. 160). It thus seems feasible to compute $\tau_{pg}(M)$ from the results of measurements of $\tau_{pg}(\mathrm{Fe})$, $\tau_{pg}(\mathrm{Si})$, $\tau_{pg}(\mathrm{Mg})$, and $\tau_{pg}(\mathrm{Ca})$, and this has been a major motivating force behind our work.

The procedures and techniques that we use for measuring τ_{pg} of simulated meteors are those developed by Friichtenicht, Slattery, and Tagliaferri (1968), with minor modifications; the equipment and data format are described in the instrumentation section and figures 7 and 8, in this paper. We will discuss the reduction of data in broad outline only, referring the reader to Becker and Friichtenicht (1971) for additional detail. Measurements are made of the integrated intensity, initial mass, and initial velocity of each simulated meteor. In order to use the integrated intensity, one may integrate the luminosity equation, replacing dm/dt by an equivalent obtained from differentiation of equation (10) and assuming a small (but not negligible) deceleration, to get

$$E_{pg} = \tau_{pg}[E_0 - E_F - \sigma^{-1}(m_0 - m_F)] \qquad (14)$$

where $E_0 = m_0 v_0^2/2$ and $E_F = m_F v_F^2/2$ are respectively the initial and final values of the kinetic energy of the particle and where $E_{pg} \equiv \int I_{pg}\, dt$. (By small deceleration we mean that τ_{pg}, which may contain a velocity dependence, is considered constant for any one simulated meteor.) The particle ablates completely, so that $E_F \approx 0$ and $m_F \approx 0$. The drag and heat transfer data presented earlier show that $\Lambda/\Gamma \approx 1$ at low velocities, from which $\sigma \approx \tfrac{1}{2}\zeta$; at high velocities, $\sigma^{-1} m_0 \ll E_0$ and can be ignored. Then,

$$\tau_{pg} = E_{pg}(E_0 - 2\zeta m_0)^{-1} \qquad \text{(low velocities)} \qquad (15a)$$

and

$$\tau_{pg} = E_{pg}/E_0 \qquad \text{(high velocities)} \qquad (15b)$$

For the particle materials used so far, $2\zeta m_0$ becomes a negligible correction above 20 to 25 km/s, and this is the velocity range at which the transition is made from one expression to the other.

Our data are acquired photometrically, and conversions must then be applied to transform them to the photographic spectral response for direct comparison with other results. The conversions necessitate a measurement of the relative spectrum $f(\lambda)$ of the emitted light. Our detector, it will be recalled, is a PMT (usually an RCA 8575) viewing through an acrylic plastic window, and it has a relative spectral response $D(\lambda)$ which extends from 3400 to 5800 Å and peaks at about 4500 Å. Because PMT spectral response functions vary among different tube types, we normalize our data to an equivalent 3400–5800 Å "flat" detector by applying the conversion factor

$$\left[\int_{3400}^{5800} f(\lambda)\, d\lambda\right] \Big/ \left[\int_{3400}^{5800} f(\lambda) D(\lambda)\, d\lambda\right] \quad (16)$$

Luminous efficiencies normalized to this "flat" response are denoted by τ_s. The τ_s data are transformed in turn to τ_{pg} according to

$$\tau_{pg} = \tau_s \left[\int_{3300}^{5200} f(\lambda) P(\lambda)\, d\lambda\right] \Big/ \left[\int_{3400}^{5800} f(\lambda)\, d\lambda\right]$$

Note that the limits of the $D(\lambda)$ and $P(\lambda)$ spectral ranges almost coincide. The probability that the emitted spectrum $f(\lambda)$ contains a strong line falling within one range and outside of the other is therefore very small, and since $f(\lambda)$ appears in both numerator and denominator of both conversion factors, they are determined primarily by $D(\lambda)$ and $P(\lambda)$, both of which are accurately known, and only weakly by $f(\lambda)$. Hence, the measurement of $f(\lambda)$ need not be very accurate, and velocity effects (which might cause the spectra of different particles to differ somewhat) can be ignored.

Spectral measurements are performed as described in the instrumentation section and figure 9 of this paper, following the method originated by Tagliaferri and Slattery (1969) when they measured the spectrum of simulated iron meteors ablating in air. The result of their measurement is reproduced in figure 14, along with a part of a natural meteor spectrum due to Millman and Cook (1959).

Another conversion which must be applied to our data is one which involves units of measurement. In the laboratory, all quantities are measured in consistent physical units, leading to a τ that is dimensionless. But meteor astronomers find it more convenient to measure m and v in cgs units and I_{pg} in magnitudes relative to a zero-magnitude meteor, and they require τ_{pg} in units of s/erg, 0-mag. The intensity I_{op} of a zero-magnitude meteor is by convention equal to the radiant flux within a "flat" 3300 to 5200 Å passband from a star of zero apparent photographic magnitude which emits a solar spectrum. Davis and Hall (1963) find that $I_{op} = 5 \times 10^9$ ergs/s, from which

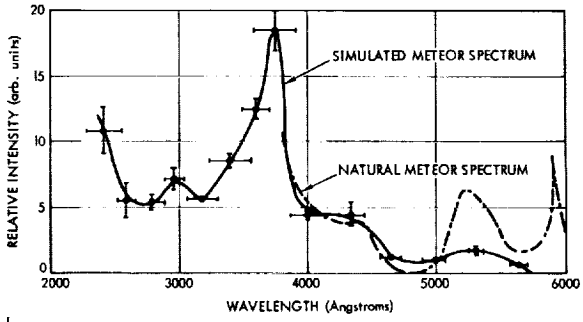

FIGURE 14.—Spectrum of iron simulated meteor in air atmosphere as measured by Tagliaferri and Slattery (1969). The natural meteor spectrum, shown for comparison, was obtained by Millman and Cook (1959).

$$\tau_{pg}(\text{physical units}) = 5 \times 10^9\, \tau_{pg}(\text{s/erg, 0-mag}) \quad (18)$$

In our most recent experiments, τ_{pg} of iron simulated meteors in an air atmosphere was measured for 167 individual particles with initial velocities ranging from 11.1 to 46.3 km/s. We also obtained τ_{pg} data for 120 copper simulated meteors in air, with initial velocities between 10.2 and 47.4 km/s. Copper, of course, is not a meteoroid constituent; rather, it was selected because it is a useful material with which to begin to examine elemental differences in luminous efficiency. Copper has an atomic mass only 10 percent greater than that of iron but a considerably different electronic structure. It has occasionally been claimed that the predominance of iron lines in low-velocity meteor spectra can be explained by the fact that iron atoms, being the heaviest of the major meteor constituents, possess a greater kinetic energy and are therefore most likely to be excited upon collisions with gas molecules. If this were a significant effect, one

would expect τ_{pg}(Cu) to exceed τ_{pg}(Fe) by ~10 percent. If τ_{pg}(Cu) and τ_{pg}(Fe) should differ widely, on the other hand, it would indicate that mass differences do not significantly contribute to differences in emission from one constituent to the next and that such differences are probably more closely involved with electronic structure.

Figures 15 and 16 present, respectively, the results of the τ_{pg}(Fe) and τ_{pg}(Cu) experiments. In each figure, the data for each 1 km/s interval of velocity have been averaged and plotted as a single point, with error bars denoting the standard deviations of the averages. The smooth curves in the figures are least-squares best fits for $v_0 \geq 18$ km/s in the case of τ_{pg}(Fe) and $v_0 \geq 14$ km/s in the case of τ_{pg}(Cu), and visually-estimated best fits at lower velocities. Values of τ_s and τ_{pg} read from these smooth curves are listed in table 4. For iron, τ_{pg}(Fe) first rises with increasing particle velocity, reaching a peak value 2.3×10^{-12} s/erg, 0-mag at $v_0 \approx 18$ km/s. At higher velocities $\tau_{pg}(\text{Fe}) \propto v_0^{-3/4}$, falling to 2.1×10^{-12} s/erg, 0-mag at 20 km/s and 1.3×10^{-12} s/erg, 0-mag at 40 km/s. The behavior of copper is somewhat similar, but there are very important differences; τ_{pg}(Cu) peaks at 13 to 14 km/s, with a peak value of only 9.5×10^{-14} s/erg, 0-mag, and thereafter $\tau_{pg}(\text{Cu}) \propto v_0^{-1/2}$, declining to 7.3×10^{-14} and 5.3×10^{-14} s/erg, 0-mag at 20 and 40 km/s. The differences are, then, that the peak velocities are not the same, that the velocity dependences in the high velocity regime differ, and, significantly, that τ_{pg}(Cu) is at least a factor of 20 lower than τ_{pg}(Fe) at any velocity between 18 and 47 km/s.

These results certainly permit one to conclude that differences in atomic mass are totally unrelated to the relative intensity of radiation emitted within the photographic spectral range from atoms of the different constituent species in a meteoroid. However, the macroscopic nature of the results do not allow any definite connections to be made between the behavior of τ_{pg} and specific details of the electronic structure of the two elements.

Interestingly enough, the data for τ_{pg}(Fe) correspond very well to predictions of Öpik (1958, p. 139) of the behavior of the visual luminous efficiency τ_v of dustball meteors with dilute comae. We demonstrate this correspondence in table 5, where the ratio τ/τ_{peak} is compared at

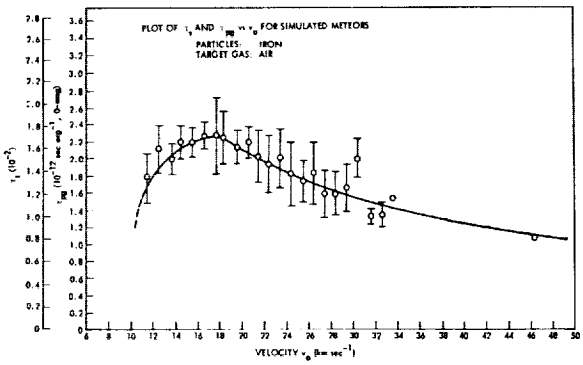

FIGURE 15.—Luminous efficiency of iron simulated meteors as a function of velocity v_0. Data for each 1 km/s velocity interval have been averaged; error bars extend ± one standard deviation of the average. When no bars are shown, the velocity interval contained only one datum.

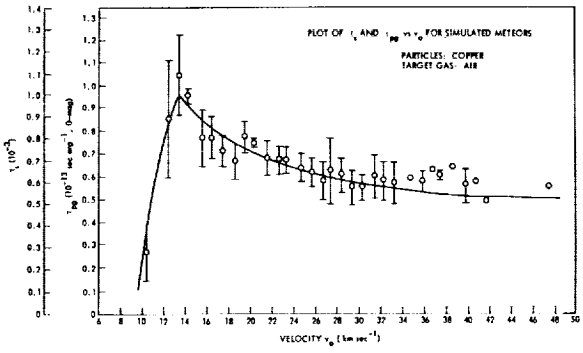

FIGURE 16.—Luminous efficiency of copper simulated meteors as a function of velocity v_0. See figure 15 for plotting and error bar conventions.

various velocities for Öpik's computation and for our experiment. We do not regard the small differences in the velocity of τ_{peak} as significant, since in both cases the peak is rather broad. The rapid rise in τ from low velocities is present in both results, and the $v^{-3/4}$ relationship at high velocities that we observed experimentally compares favorably with Öpik's predicted velocity exponent, which is −0.88.

Perhaps the most significant findings from this experiment appear when the data for τ_{pg}(Fe) are replotted in the log-log presentation employed by Ayers et al. (1970) in reporting their artificial meteor results. Such a plot appears in figure 17, where we have included for direct comparison

TABLE 4.—*Values of τ_s and τ_{pg} for Iron and Copper Micrometeors*[a]

Velocity (km/s)	Iron		Copper	
	τ_s (physical)	τ_{pg} (s/erg, 0 mag)	τ_s (physical)	τ_{pg} (s/erg 0 mag)
10	—	—	0.00026	2.6×10^{-14}
11	0.0115	1.5×10^{-12}	0.00057	5.6×10^{-14}
12	0.0133	1.8×10^{-12}	0.00079	7.8×10^{-14}
14	0.0155	2.1×10^{-12}	0.00096	9.5×10^{-14}
16	0.0168	2.2×10^{-12}	0.00087	8.5×10^{-14}
18	0.0170	2.3×10^{-12}	0.00080	7.8×10^{-14}
20	0.0159	2.1×10^{-12}	0.00074	7.3×10^{-14}
22	0.0149	2.0×10^{-12}	0.00070	6.9×10^{-14}
24	0.0140	1.9×10^{-12}	0.00067	6.6×10^{-14}
26	0.0132	1.8×10^{-12}	0.00064	6.3×10^{-14}
28	0.0125	1.7×10^{-12}	0.00062	6.1×10^{-14}
30	0.0118	1.6×10^{-12}	0.00060	5.9×10^{-14}
32	0.0112	1.5×10^{-12}	0.00058	5.7×10^{-14}
34	0.0107	1.4×10^{-12}	0.00057	5.6×10^{-14}
36	0.0103	1.4×10^{-12}	0.00055	5.4×10^{-14}
38	0.0098	1.3×10^{-12}	0.00054	5.3×10^{-14}
40	0.0094	1.3×10^{-12}	0.00054	5.3×10^{-14}
42	0.0091	1.2×10^{-12}	0.00053	5.2×10^{-14}
44	0.0088	1.2×10^{-12}	0.00053	5.2×10^{-14}
46	0.0085	1.1×10^{-12}	0.00053	5.2×10^{-14}

[a] Data taken from smooth curves, figures 15 and 16.

TABLE 5.—*Values of Normalized Luminous Efficiency Measured for Iron and Predicted for Dustball Meteors*

Velocity (km/s)	Dustballs[a] $\tau_v/\tau_v(peak)$	Iron[b] $\tau_{pg}/\tau_{pg}(peak)$
10.4	0.71	~0.47[c]
14.8	1.00	0.95
18.0	—	1.00
20.9	0.96	0.90
29.6	0.64	0.70
41.8	0.45	0.53
59.2	0.37	~0.41[d]

[a] Data from Öpik (1958).
[b] Data from current experiment.
[c] Visual extrapolation.
[d] Extrapolation assuming $\tau_{pg}(\mathrm{Fe}) \propto v^{-3/4}$.

both the Ayers et al. results and also data for Harvard Meteors 1242 and 19816 as reduced by Cook et al. (1963). Both of these meteors are believed to be of asteroidal origin; in order to place them on the same scale as the $\tau_{pg}(\mathrm{Fe})$ data, we have plotted both natural meteor points in terms of $\tau_{pg}(M)/A_{\mathrm{Fe}}$, using the value of $\tau_{pg}(M)$ given by Cook et al. and $A_{\mathrm{Fe}}=0.15$ from Öpik (1958). Considering that our $\tau_{pg}(\mathrm{Fe})$ data are accurate to ±40 percent or better and that Ayers et al. quote uncertainties for theirs in the 15 to 25 percent range, we regard the agreement between the simulated meteor and artificial meteor results as excellent. Reasonable agreement with the two natural meteor points also exists. Since the artificial meteor data (and, of course, the natural meteor data) were obtained from actual entry of bodies into the Earth's atmosphere, we believe that the agreement shown in figure 17 is extremely strong evidence that our procedures properly simulate natural meteor processes.

The reader will have noted that our observations of the velocity dependence of $\tau_{pg}(\mathrm{Fe})$ differ rather markedly from at least some current beliefs about the velocity dependence of $\tau_{pg}(M)$. The latter has been studied through the statistical

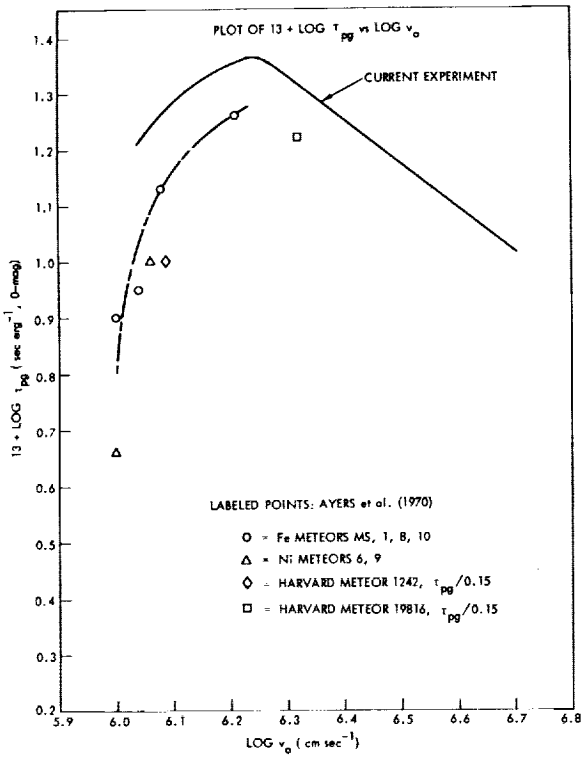

FIGURE 17.—Log τ_{pg} as a function of log v_0. Data from the currently-described experiment (Becker and Friichtenicht, 1971) are compared with artificial meteor results (Ayers et al., 1970) and two natural meteor data points (Cook et al., 1963); for the latter, τ_{pg} has been divided by 0.15, the relative abundance of iron in meteoritic stone, to permit a comparison with τ_{pg}(Fe).

analysis of meteor observations by Ceplecha and Padevět (1961) and Verniani (1965), who reached different conclusions; these have been debated at some length by Verniani (1965, 1970), Ceplecha (1966, 1968), and various others. We do not wish to join this debate at the present time. However, it is necessary to point out that the failure of τ_{pg}(Fe) to behave as a function of velocity according to Verniani's thesis that $\tau_{pg}(M) \propto v$, or according to any other proposed velocity dependence of $\tau_{pg}(M)$, is not an argument against either the accuracy or the relevance of our results. If, as we believe, equation (13) is valid, then it is neither necessary or even likely that the functional dependence of $\tau_{pg}(M)$ on velocity be the same as that of any one $\tau_{pg}(k)$. As one hypothesis, if $\tau_{pg}(k)$ of the lighter meteor constituents (which are known to emit more strongly from high velocity meteors) should behave similarly to τ_{pg}(Fe) except to peak at higher velocities, a superposition of them and τ_{pg}(Fe) could easily lead to a $\tau_{pg}(M)$ that is roughly proportional to v over a major part of the meteor velocity spectrum. There is some highly preliminary supporting evidence for such a hypothesis in our results, since τ_{pg}(Fe) was found to peak at a higher velocity than τ_{pg}(Cu).

We are presently preparing to extend our experiments to other materials with the intent of investigating some of these possibilities. One planned experiment is to check the validity of equation (13) by measuring separately the luminous efficiencies of titanium and the compound $FeTiO_3$. Since oxygen does not radiate within the photographic spectral range, we would expect to find that $\tau_{pg}(FeTiO_3) = 0.37\tau_{pg}(Fe) + 0.32\tau_{pg}(Ti)$ if equation (13) holds. Provided that this experiment proves successful, we will then attempt to measure τ_{pg}(Si), τ_{pg}(Mg), and τ_{pg}(Ca), after which we would be able to compute $\tau_{pg}(M)$ as proposed earlier.

Ionization

The ionized wakes produced by ablating meteoroids are known to be responsible for radiometeor phenomena. In recent years the study of these phenomena has been improved to the point where radiometeor observations have become an important research tool, complementing photographic observational methods. Moreover, the formation of the ionized wake is another basic mechanism of energy transfer from the meteoroid to the atmosphere and must therefore be understood before the description of the energy transfer process can be considered complete.

Meteor ionization can be treated in terms of the fraction of the meteoroid kinetic energy that is expended in ion-electron pair production, leading to an equation analogous to the luminosity equation (11):

$$I_q = -\tfrac{1}{2}\tau_q v^2 \, dm/dt \qquad (19)$$

where I_q is the energy per unit time expended in ionization and τ_q is the ionizing efficiency. In the case of ionization, however, it is more convenient to deal with the electron line density $\alpha = I_q/\phi v$,

where ϕ is the mean energy required to create a single ion-electron pair. A still more fundamental quantity is the probability β that a single meteoroid atom will produce an ion-electron pair as a result of a collision with an atmospheric molecule before the former has been reduced to thermal energy. The ionization probability and electron line density are related according to

$$\alpha = -(\beta/\mu v)(dm/dt) \qquad (20)$$

in which μ is the mean mass of a meteoroid atom, from which it follows that

$$\tau_q = (2\phi/\mu v^2)\beta \qquad (21)$$

The radiometeor problem essentially reduces to the need for an evaluation of β, since ϕ and μ are known for all meteoroid constituents. Once this is accomplished, radiometeor measurements of α and v would permit the meteoroid mass to be found.

Our remarks at the beginning of the luminosity discussion regarding the difficulty of obtaining τ_{pg} from theoretical first principles apply to ionization as well, although here the problems are not quite as complex. Predictions of τ_q and/or β based on the theory of collisional ionization have been offered by, among others, Öpik (1958), Derbeneva (1966), Furman (1967), and Sida (1969). The deduction of τ_q from observational data has been attempted by Verniani and Hawkins (1964), whose method required the simultaneous photographic and radio observation of the meteors. Their results appear to lead to a current reasonable best estimate of β for cometary meteors, but they suffer from the combined errors and uncertainties in both observational techniques (notable among which is the uncertainty in τ_{pg}). The most recent review of the subject to have come to our attention is by Verniani (1970); in it the author examines a number of theoretical and experimental results and concludes that the best estimate derived by himself and Hawkins, namely that

$$\beta/\mu = 2.6\times10^{-6}\, v^4 \qquad \text{(cgs units)} \qquad (22)$$

should continue to be used in radiometeor data reduction. As in the case of luminosity, our work is not of a type that would lead us directly to challenge any value of β proposed for composite meteoroids by others; we will, however, permit ourselves to observe that in our view, β is still sufficiently unknown that any proposed value is probably best regarded as an estimate only until much better data become available.

The basic approach that we have taken to the study of ionization probability through the medium of simulated meteor experiments is the same as that pursued in our luminosity work: to evaluate β from a series of experiments in which monoconstituent particles are made to interact with air and monoconstituent gases, in the hope that the results will lead to a firmer knowledge of the behavior of β for different single elements and may eventually allow a β for multiconstituent meteoroids to be derived therefrom. The experimental techniques employed were described in the instrumentation section and figures 10 and 11; they were developed by Slattery and Friichtenicht (1967), who were the first to measure β for simulated meteoroids. The concept of this kind of experiment and the reduction of the data are both relatively simple. We operate only with initial velocities in excess of 20 to 25 km/s, where, as we already saw, deceleration can be neglected. The total charge Q due to ions is collected in an ionization chamber. The energy per particle atom is low enough that all ions can be assumed singly charged, so that N_I, the total number of ion-electron pairs created, is equal to Q/e, where e is the electron charge. The mass μ of a particle atom is known and the initial mass m_0 is measured prior to the start of ablation, and thus the total number of particle atoms N_A can be found as the ratio m/μ. The ionization probability is then computed from

$$\beta = N_I/N_A \qquad (23)$$

To date, simulated meteor measurements of β have been reported by Slattery and Friichtenicht (1967) for iron particles interacting with air and argon, and by Friichtenicht and Becker (1971) for copper and lanthanum hexaboride (LaB_6) particles interacting with air. The choice of the latter two materials may seem strange until it is recalled why copper was selected for comparison with iron in our luminosity studies; the same criteria apply here as well. Lanthanum hexaboride was selected for two reasons: First, at the time the experiments were performed, it was the only compound that had been successfully accelerated

to meteoric velocities (now, however, see tables 1 and 2), and we were anxious to observe the behavior of a compound material. Second, it had been discovered that LaB_6 particles often achieved velocities in excess of 100 km/s, and it was, we felt, highly desirable to examine the velocity dependence of β at extreme velocities. Most prior theoretical and observational treatments have had as their result $\beta \propto v^n$, with n at least $+2$ and possibly as large as $+5$. One might expect that at some limiting velocity β would become proportional to v^2, i.e., to energy of the projectile atom. A transition to a $\beta \propto v^2$ law had not previously been observed for any material, and there was a chance that such a transition could be detected in LaB_6 ionization.

Figures 18, 19, and 20 show, respectively, the simulated meteor results obtained for β(Fe), β(Cu), and $\beta(LaB_6)$ as functions of particle velocity v_0 measured just prior to the entrance of the particle into the gas. Each figure also shows a straight line fit to the data by least squares for $20 \leq v_0 \leq 45$ km/s in figure 18; $16 \leq v_0 \leq 38$ km/s in figure 19; and $20 \leq v_0 \leq 112$ km/s in figure 20. The equations of the least-squares fits (velocity in cm/s in all cases) are

$$\beta(\mathrm{Fe}) = 1.50 \times 10^{-21} v_0^{3.12} \qquad (24a)$$

found by Slattery and Friichtenicht, and

$$\beta(\mathrm{Cu}) = 2.17 \times 10^{-35} v_0^{5.24} \qquad (24b)$$

and

$$\beta(\mathrm{LaB_6}) = 6.31 \times 10^{-21} v_0^{3.08} \qquad (24c)$$

found by Friichtenicht and Becker. The above may be compared to the result of Verniani and Hawkins (1964) for β of cometary meteors:

$$\beta(\mathrm{com}) = 1.0 \times 10^{-28} v_0^{4.0} \qquad (25)$$

obtained from equation (22) by assuming an average meteoroid atom to have a mass $\mu = 23$.

The obvious functional similarity between β(Fe) and $\beta(LaB_6)$ is not repeated with β(Cu), but it is nevertheless interesting that in the important 20 to 40 km/s velocity range, the ionization probabilities of iron, copper, and LaB_6 do not differ very greatly. Respective values are 0.07, 0.02, and 0.16 at 20 km/s; 0.24, 0.19, and 0.56 at 30 km/s; and 0.60, 0.85, and 1.36 at 40 km/s.

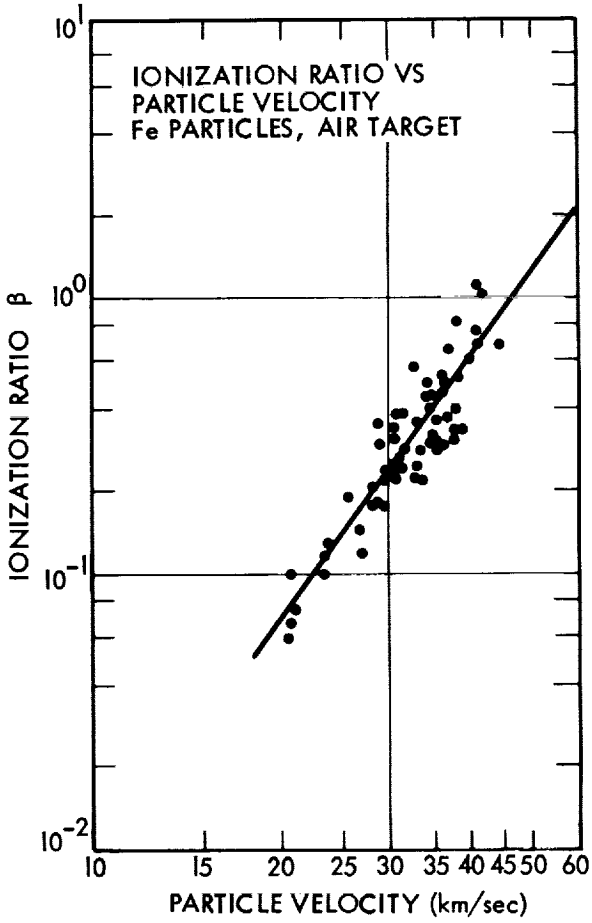

FIGURE 18.—Ionization probability of iron-simulated meteors as a function of v_0. Data are from Slattery and Friichtenicht (1967). Straight line shown has been fit by least squares; its equation is $\beta(\mathrm{Fe}) = 1.50 \times 10^{-21} v_0^{3.12}$

The LaB_6 results at very high velocities appear to have some rather interesting features. One is that the least-squares fit expressed by equation (24c) seems to hold even at 112 km/s, and there is no evidence that β is approaching a proportionality to v^2 at this high a velocity. Another is that $\beta(LaB_6)$ clearly exceeds unity at high velocities and attains a value as large as 50 at 112 km/s. An ionization "probability" greater than unity requires an other-than-probabilistic interpretation; in our usage as defined by equation (23), it means that some ablated meteoroid molecules suffer more than one ionizing collision with atoms or molecules of the atmospheric gas and that it is the latter that undergo ionization.

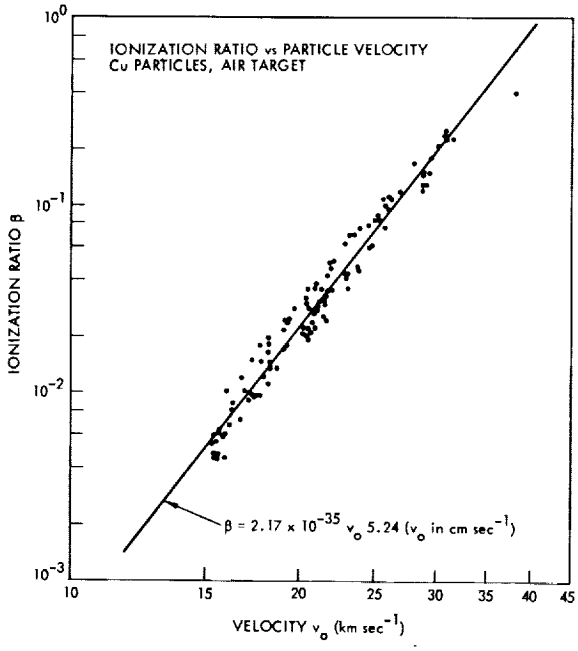

FIGURE 19.—Ionization probability of copper simulated meteors as a function of v_0. Data are from Friichtenicht and Becker (1971). Least-squares fit is shown.

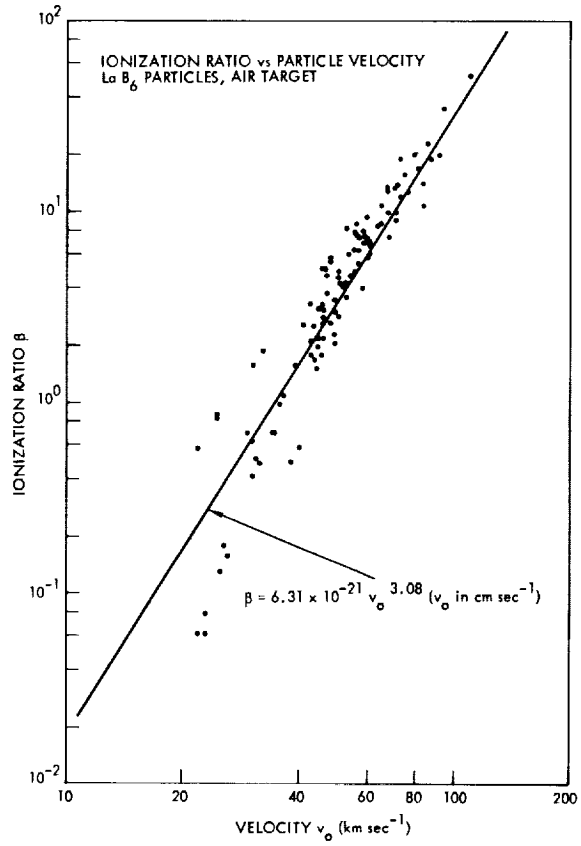

FIGURE 20.—Ionization probability of lanthanum hexaboride simulated meteors as a function of v_0. Data are from Friichtenicht and Becker (1971). Straight line with equation shown is a least-squares fit. As noted in text, separate least-squares fits were attempted above and below 40 km/s, but the results were the same within the accuracy of the experiment.

Friichtenicht and Becker (1971) support this conclusion in a discussion of the possible influence of competing energy exchange mechanisms.

At present, most theories of meteor ionization do not appear to consider either atmospheric ionization in general or the possibility of ionization of multiple atmospheric atoms by a single projectile atom in particular as likely. Instead, the theories usually regard the projectile atom as the one undergoing ionization (in some cases, multiple ionizations), primarily because of the fact that in the meteor problem, the projectile atom almost always has a lower first ionization potential. Although 112 km/s is considerably above the highest velocity that cometary meteors attain, $\beta(LaB_6)$ is still greater than unity for $40 \leq v_0 \leq 70$ km/s, and these are velocities which are possible for natural meteors. There may be, then, a need for some modification of current meteor ionization theory at high velocities.

It should be noted here that Friichtenicht, Slattery, and Hansen (1967) have extended the simulated meteor ionization experiments to a wide variety of other gases, from which they obtain a considerable amount of information that may prove useful in the study of collisional ionization on the atomic scale. In this sense the simulated meteor becomes a form of atomic beam. This work will not be discussed here because its immediate relevance to the gross behavior of meteors is slight; however, it has opened some interesting possibilities for new methods of experimentally studying atomic interactions.

We are not particularly concerned that our results for β are consistently larger than those that seem to be regarded as appropriate to cometary meteors, since we feel that the situation may be

similar to the problem of the velocity dependence of τ_{p0}. The weighting factors that would have to be applied to elemental β values in order to synthesize a β for a meteoroid are as yet unknown, and for this reason we think that it is too early to conclude that our results are in any way inconsistent. We continue to believe that such a synthesis is possible and that it would be preferable in many respects to the assumption of an "average" meteoroid atom as is now done in reducing observational material. However, just as the interpretation of radiometeor observations is less advanced than that of photographic observations (cf. Verniani, 1970), so too is the interpretation of simulated meteor ionization experiments less advanced than that of the luminosity experiments. Now in the planning stage are experiments designed to measure β for silicon, magnesium, and various other materials, which may provide information helpful in improving that interpretation.

CONCLUSIONS

Throughout this paper we have attempted to concentrate on basic methods and techniques for accelerating microparticles to meteoritic velocities and for employing these particles in practical simulated meteor experiments. In addition, we have presented the results of those experimental efforts which seem to us especially relevant to a number of unresolved problems in the study of meteors. Of these, primary emphasis has been given to luminosity experiments, because in this area our results as of the present time are most complete and most easily compared to natural meteor observations and to the work of other experimenters. However, we believe that our experimental work with meteor ionization may prove to be of equal or greater ultimate significance, largely because of the fact that the study of ionization seems to be generally less developed at this time than that of luminosity.

We have taken some pains to point out that the principal task which we have set for ourselves is the acquisition of basic data relating to the behavior of macroscopic particles ablating under meteoric conditions. Although we attempt to reproduce those conditions as accurately as possible in terms of flow regimes and other phenomena encountered by the particle, there is no attempt to reproduce a meteoroidal composition in the particle. For this reason it is seldom desirable or correct to compare our results directly to natural meteor observations, nor, do we feel, is it correct to imply the existence of errors in our work solely on the basis of lack of agreement when such a comparison is made. Instead, we regard our data as being most useful for two other purposes. One is to obtain a better understanding of meteoric processes and phenomena by examining them on a simpler and more controlled basis. The other is to acquire information from which values of meteoric constants defined in the theory may be synthesized.

Finally, throughout these discussions we have presented evidence which appears strongly to support our contention that meteoric processes are in fact accurately simulated in the experiments. We have noted that drag coefficients and heat transfer coefficients determined for simulated meteors are reasonable in themselves and are consistent with hypothesized ablation mechanisms and gas flow conditions. We have also discussed the agreement between our determination of τ_{p0}(Fe) and that found from artificial meteor experiments involving actual atmospheric entry of various bodies.

In closing, the authors wish to thank M. Dubin for his considerable support and encouragement of our work.

REFERENCES

ALLEN, C. W., 1955. *Astrophysical Quantities*, 1st ed., Athlone Press, London, 178.

AYERS, W. G., MCCROSKY, R. E., AND SHAO, C. -Y., 1970. Photographic observations of 10 artificial meteors, *Smithson. Astrophys. Obs. Spec. Rept.*, No. 317.

BECKER, D. G., AND FRIICHTENICHT, J. F., 1971. Measurement and interpretation of the luminous efficiencies of iron and copper simulated micrometeors, *Astrophys. J.*, **166**, 699–716.

BECKER, D. G., FRIICHTENICHT, J. F., HAMERMESH, B., AND LANGMUIR, R. V., 1965. Variable-frequency radially-stable micrometeoroid accelerator, *Rev. Sci. Instr.*, **36**, 1480–1481.

CEPLECHA, Z., 1966. Dynamic and photometric mass of meteors, *Bull. Astrom. Inst. Czech.*, **17**, 347–354.

——, 1968. Discrete levels of meteor beginning height, *Smithson. Astrophys. Obs. Spec. Rept.*, No. 279.

CEPLECHA, Z., AND PADEVĚT, V., 1961. The beginning of rapid evaporation of meteors of different dimensions, *Bull. Astrom. Inst. Czech.*, **12**, 191–195.

COOK, A. F., JACCHIA, L. G., AND MCCROSKY, R. E., 1963. Luminous efficiency of iron and stone asteroidal meteors, *Smithson. Contrib. Astrophys.*, **7**, 209–220.

DAVIS, J., 1963. On the color index of meteors, *Smithson. Contrib. Astrophys.*, **7**, 233–236.

DAVIS, J., AND HALL, J. E., 1963. Meteor luminosity and ionization, *Proc. Roy. Soc. London, A*, **271**, 120–128.

DERBENEVA, A. D., 1966. Ionization coefficient for meteoritic atoms, *Geomagnetizm i Aeronomiya*, **6**, 455–457.

FRIICHTENICHT, J. F., 1962. Two-million-volt electrostatic accelerator for hypervelocity research, *Rev. Sci. Instr.*, **33**, 209–212.

——, 1969. Evaporation of high-velocity particles in free-molecule flow, *J. Am. Inst. Aeronaut. Astronaut.*, **7**, 598–601.

FRIICHTENICHT, J. F., AND BECKER, D. G., 1971. Measurements of the ionization probability of Cu and LaB_6 simulated micrometeors, *Astrophys. J.*, **166**, 717–724.

FRIICHTENICHT, J. F., SLATTERY, J. C., AND HANSEN, D. O., 1967. Ionization from Fe atoms incident on various gas targets, *Phys. Rev.*, **163**, 75–80.

FRIICHTENICHT, J. F., SLATTERY, J. C., AND TAGLIAFERRI, E., 1968. A laboratory measurement of meteor luminous efficiency, *Astrophys. J.*, **151**, 747–758.

FURMAN, A. M., 1967. Meteor trail ionization theory, IV. Ionization efficiency through collision of vaporized meteoroid particles with air molecules, *Astron. Zh.*, **10**, 844–853.

HANSEN, D. O., AND ROY, N. L., 1966. A solid-state low-noise preamplifier, *Nucl. Instr. Methods*, **40**, 209–212.

HERSH, A. S., FRIICHTENICHT, J. F., AND SLATTERY, J. C., 1969. Drag coefficients of microscopic spheres in free molecule flow, in *Rarefied Gas Dynamics*, edited by L. Trilling and H. Y. Wachman, Academic Press, New York, **1**, 757–766.

HIRSCHFELDER, J. O., CURTISS, C. F., AND BIRD, R. B., 1954. Molecular theory of gases and liquids, J. Wiley and Sons, Inc., New York, Ch. 1.

MCCROSKY, R. E., AND SOBERMAN, R. K., 1963. Results from an artificial iron meteoroid at 10 km/sec, *Smithson. Contrib. Astrophys.*, **7**, 199–208.

MILLMAN, P. M., 1963. A general survey of meteor spectra, *Smithson. Contrib. Astrophys.*, **7**, 119–127.

MILLMAN, P. M., AND COOK, A. F., 1959. Photometric analysis of a spectrogram of a very slow meteor, *Astrophys. J.*, **130**, 648–662.

ÖPIK, E. J., 1933. Atomic collisions and radiation of meteors, *Acta et Commental. Univ. Tartu* (Dorpat), **A26**, No. 2.

——, 1955. Meteor radiation, ionization, and atomic luminous efficiency, *Proc. Roy. Soc. London, A*, **230**, 463–501.

——, 1958. *Physics of Meteor Flight in the Atmosphere*, Interscience Publishing Co., New York, 174 pp.

ROY, N. L., AND BECKER, D. G., 1971. A time interval selector and proportional delay generator, *Rev. Sci. Instr.*, **42**, 204–209.

SEARES, F. H., AND JOYNER, M. C., 1943. Effective wave lengths of standard magnitudes; color temperature and spectral type, *Astrophys. J.*, **98**, 302–330.

SHELTON, H., HENDRICKS, C. D., JR., AND WUERKER, R. F., 1960. Electrostatic acceleration of microparticles to hypervelocities, *J. Appl. Phys.*, **31**, 1243–1246.

SIDA, D. W., 1969. The production of ions and electrons by meteoric processes, *Monthly Notices Roy. Astron. Soc.*, **143**, 37–47.

SLATTERY, J. C., AND FRIICHTENICHT, J. F., 1967. Ionization probability of iron particles at meteoric velocities, *Astrophys. J.*, **147**, 235–244.

SLATTERY, J. C., FRIICHTENICHT, J. F., AND HAMERMESH, B., 1964. Interaction of micrometeorites with gaseous targets, *J. Am. Inst. Aeronaut. Astronaut.*, **2**, 543–548.

TAGLIAFERRI, E., AND SLATTERY, J. C., 1969. A spectral measurement of simulated meteors, *Astrophys. J.*, **155**, 1123–1127.

VERNIANI, F., 1965. On the luminous efficiency of meteors, *Smithson. Contrib. Astrophys.*, **8**, 141–172.

——, 1970. Structure and fragmentation of meteoroids, *Space Sci. Rev.*, **10**, 230–261.

VERNIANI, F., AND HAWKINS, G. S., 1964. On the ionizing efficiency of meteors, *Astrophys. J.*, **140**, 519–564.

WHIPPLE, F. L., AND HAWKINS, G. S., 1959. Meteors, *Handbuch der Physik.*, **52**, 519–564.